Characterization of the small *Arabidopsis thaliana* GTPase and ADP-ribosylation factor-like 2 protein TITAN5

Inga Mohr[1], Amin Mirzaiebadizi[2], Sibaji K. Sanyal[1], Pichaporn Chuenban[1], Mohammad R. Ahmadian[2], Rumen Ivanov[1] and Petra Bauer[1,3]

[1]Institute of Botany, Heinrich Heine University, 40225 Düsseldorf, Germany.
[2]Institute of Biochemistry and Molecular Biology II, Medical Faculty and University Hospital Düsseldorf, Heinrich Heine University, Düsseldorf, Germany
[3]Cluster of Excellence on Plant Sciences, Heinrich Heine University, 40225 Düsseldorf, Germany.

Author contributions: I.M., M.R.A., R.I., and P.B. conceived the project; I.M., A.M., S.K.S., P.C., M.R.A., R.I. and P.B. designed experiments, supervised the research and analyzed data; I.M., A.M., S.K.S., and P.C. performed experiments and analyzed data; I.M. wrote the manuscript; I.M., A.M., M.R.A., R.I., and P.B. edited the manuscript; P.B. acquired funding. R.I. and P.B. agreed to serve as the author responsible for contact and communication.

Highlights

- The small ARF-like GTPase TTN5 has a very rapid intrinsic nucleotide exchange capacity with a conserved nucleotide switching mechanism
- Biochemical data classified TTN5 as a non-classical small GTPase, likely present in GTP-loaded active form in the cell
- YFP-TTN5 is dynamically associated with vesicle transport and different processes of the endomembrane system, requiring the active form of TTN5

Running title

ARF-like GTPase TTN5 functions

Abstract

Small GTPases comprise key proteins in signal transduction that function by conformational switching ability between GDP- and GTP-bound states. The ADP-ribosylation factor (ARF) family is involved in vesicle trafficking and cellular functions. Though evolutionarily well conserved, little is known about ARF and ARF-like GTPases in plants. Here, we characterized functional properties and cellular localization of the essential small ARF-like GTPase TITAN5/HALLIMASCH/ARL2/ARLC1 (hereafter termed TTN5) from *Arabidopsis thaliana*. TTN5 showed rapid guanine nucleotide exchange capacity comparable to that of human counterparts, but a remarkably low GTP hydrolysis reaction. A TTN5^{Q70L} mutant had enhanced nucleotide exchange activity, indicative of intracellular activation, while TTN5^{T30N} with fast nucleotide dissociation can be considered a dominant-negative form. This suggests that TTN5 is present in GTP-loaded active form in the cells. YFP-tagged TTN5 and the two derived mutant variants were located at multiple sites of the endomembrane system in the epidermis of Arabidopsis seedlings and *Nicotiana benthamiana* leaves. While YFP-TTN5 and YFP-TTN5^{Q70L} were highly mobile in the cells, mobility was reduced for TTN5^{T30N}. Colocalization with endomembrane markers in combination with pharmacological treatments resolved localization at membrane sites and showed that YFP-TTN5 and YFP-TTN5^{Q70L} were located in Golgi stacks, multivesicular bodies, while this was less the case for YFP-TTN5^{T30N}. On the

other hand, all three TTN5 forms were located at the plasma membrane. Hence, the unusual capacity of rapid nucleotide exchange activity of the small ARF-like GTPase TTN5 is linked with cell membrane dynamics, likely associated with vesicle transport pathways in the endomembrane system.

Keywords

TTN5; ARF-like; ARL2; endomembrane; GTPase; plasma membrane; vesicle

Abbreviations

Arabidopsis	*Arabidopsis thaliana*
ARF-like / ARL	ADP-ribosylation factor-like
BFA	brefeldin A
EE	early endosomes
GAP	GTPase-activating protein
GEF	guanine nucleotide exchange factor
ICQ	intensity correlation quotient
MVB	multivesicular body
TGN	*trans*-Golgi network
TTN5	TITAN 5

Introduction

A large variety of regulatory processes in signal transduction depends on guanine nucleotide-binding proteins of the GTPase family. Following the identification of common oncogenes (*HRAS, KRAS,* and *NRAS*) a new class of GTPases has been recognized, that became known as the RAS superfamily of small GTPases (Bos, 1988; Hall, 1990; Kahn et al., 1992). RAS proteins have many conserved members in the eukaryotic kingdom. The RAS superfamily consists of five subfamilies in mammals: the Rat sarcoma (RAS), RAS homologs (RHO), RAS-like proteins in the brain (RAB), Ras-related nuclear proteins (RAN), and ADP-ribosylation factor (ARF) subfamilies (Kahn et al., 1992; Ahmadi et al., 2017). In *Arabidopsis thaliana* (Arabidopsis) only four families are represented, the ROP (Rho of plants), RAB, RAN, and the ARF (Vernoud et al., 2003). The subfamilies are classified by sequence identity and characteristic sequence motifs with well-conserved regulatory functions within the cell (Kahn et al., 1992). Many mammalian small GTPases have been shown to act as molecular switches in signal transduction. They switch from inactive GDP-loaded to active GTP-loaded GTPase form. The different activity states enable them to form differential complexes with proteins or act in tethering complexes to the target membrane. Small GTPases have usually low intrinsic GDP/GTP exchange and GTP hydrolysis activity and require the regulation by guanine nucleotide exchange factors (GEFs) and GTPase-activating proteins (GAPs). GEFs are potentially recruited to the inactive, GDP-bound GTPase at their site of action and accelerate GDP/GTP exchange leading to GTPase activation. GTP binding induces a conformational change of two regions referred to as switch I and II. The active, GTP-loaded GTPases exert their function *via* direct interaction with their effectors (Sztul et al., 2019; Nielsen, 2020; Adarska et al., 2021) until their inactivation by GAPs, which stimulate the hydrolysis of GTP. Most of the known protein interactions important for their signaling functions occur in the active conformation of the GTPases. Members of the ARF family contain a conserved glycine at position 2 (Gly-2) for the characteristic *N*-myristoylation of an amphipathic helix (Kahn et al., 1992). ARF GTPases are often involved in vesicle-mediated endomembrane trafficking in mammalian cells and yeast (Just and Peränen, 2016).

In plants, the activities of small GTPases and their functional environments in the plant cells are by far not understood well and only described in a very rudimentary manner. In particular, the ARF family of small GTPases is surprisingly poorly described in plants, although the Arabidopsis ARF family consists of twelve ARF, seven ARF-like, and the associated SAR1 proteins (Singh et al., 2018). The best-studied plant ARF-GTPases, SAR1 and ARF1, act in the anterograde and retrograde vesicle transport between the endoplasmic reticulum (ER) and the Golgi. SAR1 is involved in COPII trafficking from the ER to the Golgi, whereas ARF1 participates in the opposite COPI pathway (Singh et al., 2018; Nielsen, 2020). Another ARF-like protein, ARL1, has perhaps a role in endosome-to-Golgi trafficking (Latijnhouwers et al., 2005; Stefano et al., 2006). This role in vesicle formation within the endomembrane system is well conserved in eukaryotes and raises the question of whether other plant ARF members are also involved in functioning of the endomembrane system. A recent study showed Golgi-related localization for some ARF and ARF-like proteins (Niu et al., 2022) promoting a general involvement of the ARF family in the endomembrane system.

TITAN5 (TTN5)/HALLIMASCH (HAL)/ARF-LIKE2 (ARL2), ARLC1, from here on referred to as TTN5, is essential in plant development. It was identified in two independent screens for abnormal embryo mutants. The *ttn5* loss-of-function mutants are arrested soon after cell division of the fertilized egg cell, without displaying a phenotype in pollen or the male gametophyte, indicating the fundamental, potentially housekeeping role in cellular activities of TTN5 protein (Mayer et al., 1999; McElver et al., 2000; Lloyd and Meinke, 2012). TTN5 is closely related in sequence to human ADP-ribosylation factor-like 2 (HsARL2). HsARL2 has high nucleotide dissociation rates, being up to 4000-fold faster compared to RAS (Hanzal-Bayer et al., 2005; Veltel et al., 2008). HsARL2 is associated with different functions in cells, ranging from microtubule development, also identified for yeast and Caenorhabditis homologs (Bhamidipati et al., 2000; Fleming et al., 2000; Radcliffe et al., 2000; Antoshechkin and Han, 2002; Tzafrir et al., 2002; Mori and Toda, 2013), adenine nucleotide transport in mitochondria (Sharer et al., 2002) and control of phosphodiesterase activity in cilia (Ismail et al., 2011; Fansa and Wittinghofer, 2016). It is thought that HsARL2 requires fast-acting nucleotide exchange and participates in different cellular processes that depend on developmental and tissue-specific factors. With regard to the plant ortholog, it is still completely unknown, which cellular roles TTN5 fulfills in plants. Until today, the function of this small plant GTPase remains elusive at the molecular level. Besides lacking knowledge of the physiological context, the GTPase characteristics and properties of the TTN5 enzyme are not yet demonstrated.

Here, we show that TTN5 is a functional small GTPase with conserved GTP hydrolysis and very fast nucleotide exchange characteristics. TTN5, based on its localization, participates in different processes in the endomembrane system. We characterized TTN5 wild type (WT) and two dysfunctional mutants (T30N and Q70L). Similar mutants have been frequently used as dominant-negative and constitutive-active forms of various GTPases (Dascher and Balch, 1994; Brumm et al., 2020; Fisher et al., 2020; Gimenez et al., 2022). This study lays the foundation for studying the functional relationships of this small GTPase.

Results

TTN5 exhibited atypical characteristics of rapid nucleotide exchange and slow GTP hydrolysis

There is a higher sequence similarity of TTN5 with its animal ARL2 ortholog than to any Arabidopsis ARF/ARL proteins (Figure 1A) (McElver et al., 2000; Vernoud et al., 2003). Several observations indicate that TTN5 plays a fundamental and essential role in cellular activities. Loss of function of TTN5 causes a very early embryo-arrest phenotype (Mayer et al., 1999;

133 McElver et al., 2000). An essential TTN5 function is also reflected by its regulation and
134 ubiquitous gene expression during plant development and in the root epidermis revealed in
135 public RNA-seq data sets of organ and single cell analysis of roots (Supplementary Figure
136 S1A-B). *TTN5* is strongly expressed during early embryo development where cell division, cell
137 elongation, and cell differentiation take place (Supplementary Figure S1C). Hence, *TTN5* is
138 expressed and presumably functional in very fundamental processes in cells with stronger
139 expression when cells grow and divide.
140 The molecular switch functions can be presumed for TTN5 (Figure 1B-C). HsARL2 has a fast
141 GDP/GTP exchange characteristic (Hanzal-Bayer et al., 2005; Veltel et al., 2008). However, it
142 had not been known whether the plant TTN5 has similar or different GTPase characteristics
143 as its animal counterparts. We characterized the nucleotide binding and GTP hydrolysis
144 properties of TTN5 and two of its mutants using heterologously expressed and purified proteins
145 and *in vitro* biochemical assays, as previously established for human GTPases ((Eberth and
146 Ahmadian, 2009) workflow in Supplementary Figure S2A-D). The mutants were T30N and
147 Q70L with amino acid exchanges in conserved positions of GTPases. The constitutively active
148 Q70L mutants can presumably not hydrolyze GTP, while the dominant-negative T30N is likely
149 to bind a GEF, preventing the latter from functioning in the proper context. Similar mutants
150 have been frequently used as dominant-negative and constitutive-active forms of various
151 GTPases (Scheffzek et al., 1997; Zhou et al., 2006; Newman et al., 2014). We monitored the
152 real-time kinetics of the interactions of fluorescent guanine nucleotides with $TTN5^{WT}$ and the
153 two potentially dysfunctional variants, $TTN5^{T30N}$ and $TTN5^{Q70L}$ using stopped-flow fluorimetry
154 (Figure 2A-C). Here, 2-deoxy-3-O-N-methylanthraniloyl-deoxy-GDP (mdGDP) and GppNHp
155 (mGppNHp), a non-hydrolyzable GTP analog, were used to mimic GDP and GTP binding to
156 TTN5 proteins. This approach allowed us to measure very fast reaction rates as characteristic
157 of small GTPases, such as HsARL2 and HsARL3 (Hillig et al., 2000; Hanzal-Bayer et al., 2005;
158 Veltel et al., 2008; Zhang et al., 2018). First, we determined the association of mdGDP and
159 mGppNHp in the presence of increasing amounts of nucleotide-free TTN5 proteins (Figure
160 2B). We found that TTN5 proteins were able to bind both nucleotides, except for mGppNHp
161 binding by $TTN5^{T30N}$ (Supplementary Figures S3A-F, S4A-E). Clearly, $TTN5^{Q70L}$ revealed the
162 highest k_{on} value for mGDP binding (0.401 $\mu M^{-1}s^{-1}$), which was nine-fold higher compared to
163 TTN5 (0.044 $\mu M^{-1}s^{-1}$) and $TTN5^{T30N}$ (0.048 $\mu M^{-1}s^{-1}$), respectively (Figure 2D; Supplementary
164 Figure S3D-F). The k_{on} values for mGppNHp binding were 2-fold lower for $TTN5^{WT}$ (0.029 μM^{-}
165 $^{1}s^{-1}$) and $TTN5^{Q70L}$ (0.222 $\mu M^{-1}s^{-1}$) compared with those for mGDP binding, respectively (Figure
166 2E; Supplementary Figure S4C, D). The differences of k_{on} for the different nucleotide binding
167 were low. However, it was noted that $TTN5^{Q70L}$ showed a 7.5-fold faster mGppNHp binding
168 than $TTN5^{WT}$. One remarkable observation was that we did not observe the kinetics of
169 mGppNHp association with $TTN5^{T30N}$ (Figure 2E). Therefore, we monitored the mGppNHp
170 fluorescence in the absence and the presence of nucleotide-free $TTN5^{T30N}$. As shown in
171 Supplementary Figure S4B, mGppNHp can bind to $TTN5^{T30N}$ so quickly that the association
172 cannot be resolved.
173 We next measured the dissociation of mdGDP and mGppNHp from the TTN5 proteins in the
174 presence of excess amounts of GDP and GppNHp, respectively (Figure 2C), and found quite
175 interesting differences (Figure 2D, E; Supplementary Figures S3G-I, S4F-H). First, $TTN5^{WT}$
176 revealed a k_{off} value (0.012 s^{-1} for mGDP) (Figure 2D, Supplementary Figure S3G), which was
177 100-fold faster as compared to those obtained for classical small GTPases, including RAC1
178 (Haeusler et al., 2006) and HRAS (Gremer et al., 2011), but quite similar to the k_{off} value of
179 ARF3 (Fasano et al., 2022). Second, the k_{off} values for mGDP and mGppNHp, respectively,
180 were in a similar range between $TTN5^{WT}$ (0.012 s^{-1} and 0.001 s^{-1}) and $TTN5^{Q70L}$ (0.025 s^{-1} and

181 0.006 s^{-1}), respectively, but differed 10-fold between nucleotides (Figure 2D, E; Supplementary
182 Figure S3G, I, S4F, H). Hence, mGDP dissociated from proteins 10-fold faster as compared
183 to mGppNHp. Third, the mGDP dissociation from $TTN5^{T30N}$ (k_{off} = 0.149 s^{-1}) was 12.5-fold faster
184 than that of $TTN5^{WT}$ and 37-fold faster than the mGppNHp dissociation of $TTN5^{T30N}$ (k_{off} = 0.004
185 s^{-1}), which are either characteristic of a dominant-negative mutation or a fast-cycling mutation
186 (Figure 2D-E; Supplementary Figure S3H, S4G).
187 The dissociation constant (k_d) is calculated from the ratio k_{off}/k_{on}, which inversely indicates the
188 affinity of the interaction between proteins and nucleotides (the higher k_d, the lower affinity).
189 Interestingly, $TTN5^{WT}$ binds mGppNHp (k_d = 0.029 µM) 10-fold tighter than mGDP (k_d = 0.267
190 µM), a difference, which was not observed for $TTN5^{Q70L}$ (k_d for mGppNHp = 0.026 µM, k_d for
191 mGDP = 0.061 µM) (Figure 2D-E). In contrast, the K_d value for the mGDP interaction with
192 $TTN5^{T30N}$ was even 11.5- and 50.6-fold lower (3.091 µM) than for $TTN5^{WT}$ and $TTN5^{Q70L}$,
193 suggesting that this mutant may have a rapid GDP/GTP exchange in cells (Figure 2D).
194 To obtain the complete GTPase cycle, the ability of TTN5 to hydrolyze GTP had to be
195 determined. Accordingly, the intrinsic GTP hydrolysis reaction was determined by incubating
196 100 µM GTP-bound TTN5 proteins at 25°C and injecting the samples at different time points
197 onto a reversed-phase HPLC column (Figure 2F; Supplementary Figure S5). The determined
198 GTP hydrolysis rates (k_{cat}) were quite unexpected in two respects (Figure 2G). First, all three
199 TTN5 protein forms showed quite similar k_{cat} values (0.0015 s^{-1}, 0.0012 s^{-1}, 0.0007 s^{-1};
200 Supplementary Figure S5). The GTP hydrolysis activity of $TTN5^{Q70L}$ was quite high and
201 unexpected (0.0007 s^{-1}). We had expected that the glutamine mutations at the corresponding
202 position as in the case of most other GTPases lead to drastic impairment of the intrinsic
203 hydrolysis and consequently to a constitutively active GTPase form in cells. Second, the k_{cat}
204 value of $TTN5^{WT}$ (0.0015 s^{-1}) although quite low as compared to other GTPases (Jian et al.,
205 2012; Esposito et al., 2019), was 8-fold lower than the previously determined k_{off} value for its
206 mGDP dissociation (0.012 s^{-1}) (Figure 2E). A fast intrinsic GDP/GTP exchange versus a slow
207 GTP hydrolysis can have drastic effects on TTN5 activity in cells under resting conditions, as
208 TTN5 can accumulate in its GTP-bound form, unlike the classical GTPase (Jaiswal et al.,
209 2013). To investigate this scenario, we pulled down GST-TTN5 protein from bacterial lysates
210 in the presence of an excess amount of GppNHp in the buffer using glutathione beads and
211 measured the nucleotide-bound form of GST-TTN5 using HPLC. As shown in Figure 2H,
212 isolated GST-TTN5 increasingly bonds GppNHp, indicating that the bound nucleotide is rapidly
213 exchanged for free nucleotide (in this case GppNHp). This is not the case for conventional
214 GTPases, which remain in their inactive GDP-bound forms under the same experimental
215 conditions.
216 In summary, the TTN5 sequence not only contains conserved regions necessary for
217 nucleotide binding but also TTN5 protein detectably binds nucleotides. Interestingly, the slow
218 intrinsic GTP hydrolysis rates in combination with the high dissociation rates for GDP indicate
219 that TTN5 tendency is to be present in a GTP-loaded form. A fast intrinsic GDP/GTP exchange
220 and a slow GTP hydrolysis can have drastic effects on TTN5 activity in cells under
221 resting/unstimulated conditions, as TTN5 can accumulate in its GTP-bound form, unlike the
222 classical GTPases (Jaiswal et al., 2013). On the other hand, the suspected constitutively active
223 $TTN5^{Q70L}$ still has intrinsic GTPase activity, while the T30N variant had a low affinity for mGDP.
224 Hence, we proved that TTN5 exhibits the typical functions of a small GTPase based on *in vitro*
225 biochemical activity studies, including guanine nucleotide association and dissociation, but
226 emphasized its divergences among the ARF GTPases by its kinetics.
227
228 **YFP-TTN5 is highly dynamic and localizes to different intracellular compartments**

229 Several ARF GTPases function in vesicle transport and are located at various membranous
230 sites linked with the endomembrane compartments in eukaryotes (Vernoud et al., 2003).
231 Localization had not been comprehensively studied for TTN5. To obtain hints where in a cell
232 TTN5 may be localized, we first created transgenic Arabidopsis lines constitutively expressing
233 YFP-tagged TTN5 (pro35S::YFP-TTN5) and its two mutant forms (negative pro35S::YFP-
234 TTN5^{T30N}, active pro35S::YFP-TTN5^{Q70L}) and investigated the localization in 6-day-old
235 seedlings in the epidermis of cotyledons, hypocotyls, root hair zone and in root tips (Figure 3A;
236 Supplementary Figure S6A). The microscopic observations were made in different planes of
237 the tissues, e.g. inside the cells across the vacuoles (Supplementary Figure 6) and underneath
238 the plasma membrane at the cell peripheries (Figure 3). We chose the investigation of YFP-
239 TTN5 in the epidermis as this is a tissue where *TTN5* was found to be expressed in plants
240 (Supplementary Figure S1B). YFP-TTN5 signals were detected in the nucleus, in the
241 cytoplasm, and at or in close proximity to the plasma membrane in the epidermal cotyledon
242 cells (Supplementary Figure S6B). The same localization patterns were found for mutant YFP-
243 TTN5 forms (Supplementary Figure S6C-D). The YFP-TTN5, YFP-TTN5^{T30N,} and YFP-
244 TTN5^{Q70L} signals were also present in a similar pattern in the stomata (Figure 3B-D). In
245 hypocotyls, intracellular localization of YFP-TTN5 and mutant forms was well observed in
246 nuclei and in close proximity to or at the plasma membrane (Supplementary Figure S6E-G).
247 Investigation of the root hair zone showed YFP signals in the cytoplasm and at the plasma
248 membrane of root hairs (Supplementary Figure S6H-J). In the root tip, YFP-TTN5 localization
249 was detectable inside the cytoplasm and in nuclei (Supplementary Figure S6K). YFP-TTN5^{T30N}
250 and YFP-TTN5^{Q70L} revealed the same localization (Supplementary Figure S6L-M). The
251 localization of YFP-TTN5, YFP-TTN5^{T30N,} and YFP-TTN5^{Q70L} inside the cytoplasm was
252 punctate indicating that the signals were present in cytosolic vesicle-like structures together
253 with free signals in the cytosol. This localization pattern was also present in leaf epidermal cells
254 and stomata of the cotyledons (Figure 3B-D), in the hypocotyls (Figure 3E-G), and in the cells
255 of the root hair zones and in the root hairs itself (Figure 3H-J). These observed structures point
256 to an association of TTN5 with vesicle and endomembrane trafficking. A closer inspection of
257 these structures over time in cotyledons presented mobility of YFP-TTN5 and mutant forms
258 within the cells (Supplementary Video Material S1A-C). Similar was the case for YFP-TTN5 in
259 hypocotyl cells (Supplementary Video Material S1D). Interestingly, the mobility of these
260 punctate structures differed within the cells when the GTPase-negative mutant YFP-TTN5^{T30N}
261 was observed (Supplementary Video Material S1E). We observed approximately half of the
262 cells within the hypocotyl with slowed-down or completely arrested movement, which was not
263 the case for YFP-TTN5 and YFP-TTN5^{Q70L} (Supplementary Video Material S1F). This loss of
264 mobility of YFP-TTN5^{T30N} may be a consequence of missing effector interaction. We did not
265 observe the blocked mobility for YFP-TTN5, YFP-TTN5^{T30N} and YFP-TTN5^{Q70L} in cells of the
266 root elongation zone (Supplementary Video Material S1G-I). No mobility of any YFP-TTN5
267 form was visible in root tip cells (Supplementary Video Material S1J-L).
268 To confirm the Arabidopsis data and to better visualize YFP-TTN5, we expressed YFP-
269 TTN5 constructs transiently in *Nicotiana benthamiana* leaf epidermis cells. We found that YFP-
270 TTN5, YFP-TTN5^{T30N,} and YFP-TTN5^{Q70L} were also all localized at or in close proximity to the
271 plasma membrane and in several cytosolic punctate structures, apart from the nucleus, similar
272 to Arabidopsis cotyledons, hypocotyls and root hair zones (Figure 3K-N). This showed that
273 YFP-TTN5 localization was similar between Arabidopsis epidermis cells and *N. benthamiana*
274 leaf epidermis. It should be noted that the 35S promoter-driven YFP-TTN5 constructs did not
275 complement the embryo-lethal phenotype of *ttn5-1*. On the other side, a triple hemagglutinin-
276 tagged HA_3-TTN5 driven by the 35S promoter did (Supplementary Figure S7A-C). We

expected the lack of complementation to be an effect of the large size of the YFP tag compared to the relatively small HA_3-tag. To verify that the localization of the YFP-TTN5 constructs is representative of a functional TTN5, we performed immunofluorescence staining against the HA_3-tag in HA_3-TTN5 seedlings and compared the localization pattern (Supplementary Figure S7D). The Alexa 488 staining reflecting HA_3-TTN5 was clearly visible in root cells and root hairs as expected. HA_3-TTN5 was mostly present in punctate structures close to the plasma membrane and in the cytosol, fitting with the YFP-TTN5 localization (Supplementary Figure S7D). Hence, we presume the correct localization of the YFP-TTN5 constructs in the various membrane-associated places in the cytosol including the plasma membrane.

Taken together, YFP-TTN5 and its mutant forms were located in multiple membrane compartments in the epidermis of different Arabidopsis organs and of *N. benthamiana* leaves. YFP-TTN5 and YFP-TTN5^{Q70L} displayed high mobility in the cells, while YFP-TTN5^{T30N} was less mobile. Altogether, these data suggest that TTN5 may have multiple functions as an active GTPase and may be associated with different intracellular structures of the endomembrane system.

YFP-TTN5 associates with components of the cellular endomembrane system

The localization of YFP-TTN5 prompted us to better resolve the membrane structures and to identify the nature of YFP-TTN5-positive cellular compartments. The endomembrane system is highly dynamic in the cell. Well-established fluorescent endomembrane markers and pharmacological treatments help to determine the nature of individual components of the system in parallel to colocalization studies with proteins of interest such as TTN5. To clarify the nature of the compartments, we conducted the colocalization experiments in *N. benthamiana* leaf epidermis where the localization pattern was similar to that in the Arabidopsis cotyledons and root epidermis, as it represents an established system for functional association of the multiple endomembrane components, allowing optimal identification of membrane structures (Brandizzi et al., 2002; Hanton et al., 2009).

At first, we investigated the endoplasmic reticulum (ER)-Golgi connection. This site is characteristic of association with small GTPases like ARF1, involved in COPI vesicle transport from Golgi to the ER (Just and Peränen, 2016). The soybean (*Glycine max*) protein α-1,2 mannosidase 1 (GmMan1) is a glycosidase that acts on glycoproteins at the *cis*-Golgi, facing the ER (Figure 4A). GmMan1-mCherry-positive Golgi stacks are visible as nearly round punctuate structures throughout the whole cell (Nelson et al., 2007; Wang et al., 2016). YFP-TTN5 and mutant variants partially colocalized with GmMan1-mCherry signals at the Golgi stacks (Figure 4B-D). Further, quantitative analysis confirmed the visible colocalization with the marker with Pearson coefficients 0.63 (YFP-TTN5), 0.65 (YFP-TTN5^{T30N}), and 0.68 (YFP-TTN5^{Q70L}) (Supplementary Figure S8A; see also similar results obtained with overlap coefficients), indicating a strong correlation between the two signals. Using object-based analysis, we detected 24 % overlapping YFP-TTN5 fluorescence signals with Golgi stacks, while YFP-TTN5^{T30N} and YFP-TTN5^{Q70L} signals only shared 16 and 15 % overlap with GmMan1-mCherry-positive Golgi stacks (Supplementary Figure S8B). Some YFP-TTN5 signals did not colocalize with the GmMan1 marker. This effect appeared more prominent for YFP-TTN5^{T30N} and less for YFP-TTN5^{Q70L}, compared to YFP-TTN5 (Figure 4B-D). Indeed, we identified 48 % GmMan1-mCherry signal overlapping with YFP-TTN5^{Q70L}-positive structures, whereas 43 and only 31 % were present with YFP-TTN5 and YFP-TTN5^{T30N} respectively (Supplementary Figure S8B), indicating a smaller amount of GmMan1-positive Golgi stacks colocalizing with YFP-TTN5^{T30N}. Hence, the GTPase-active TTN5 forms are likely more present at *cis*-Golgi stacks compared to dominant negative TTN5^{T30N}.

325 Next, we confirmed the Golgi localization by brefeldin A (BFA) treatment, a commonly used
326 tool in cell biology for preventing dynamic membrane trafficking events and vesicle transport
327 involving the Golgi. BFA is a fungal macrocyclic lactone that leads to a loss of *cis*-cisternae
328 and accumulation of Golgi stacks, known as BFA-induced compartments, up to the fusion of
329 the Golgi with the ER (Figure 4E). The action of BFA causes a corresponding redistribution of
330 GmMan1-mCherry (Ritzenthaler et al., 2002; Wang et al., 2016). We found that upon BFA
331 treatment, GmMan1-mCherry was present in the ER and in BFA-induced compartments. YFP-
332 TTN5 proteins showed partially matching localization with GmMan1-mCherry upon BFA
333 treatment proving the connection of TTN5 to Golgi localization (Figure 4F-H). Hence, the
334 colocalization with GmMan1-mCherry and BFA treatment confirmed the localization of TTN5
335 with the Golgi stacks and the lower association of both mutant forms with this membrane
336 compartment.
337 Second, we investigated localization to the endocytic compartments, endosomes of the
338 *trans*-Golgi network (TGN), and multivesicular bodies (MVBs) using the marker RFP-ARA7
339 (RABF2B), a small RAB-GTPase present there (Kotzer et al., 2004; Lee et al., 2004; Stierhof
340 and El Kasmi, 2010; Ito et al., 2016) (Figure 4I). These compartments play a role in sorting
341 proteins between the endocytic and secretory pathways, with MVBs developing from the TGN
342 and representing the final stage in transport to the vacuole (Valencia et al., 2016; Heucken
343 and Ivanov, 2018). Colocalization studies revealed that YFP-TTN5 protein was present at
344 RFP-ARA7-positive MVBs (Figure 4J). Noticeably, overlaps between RFP-ARA7 and YFP-
345 TTN5^{T30N} fluorescence signals were lower than for the other forms (Figure 3K-L;
346 Supplementary Figure S8C-D). We obtained a Pearson coefficient for YFP-TTN5 and YFP-
347 TTN5^{Q70L} together with RFP-ARA7 of 0.78, whereas a coefficient of only 0.59 was obtained
348 with YFP-TTN5^{T30N} confirming the visual observation (Supplementary Figure S8C; see also
349 similar results for overlap coefficients). Object-based analysis showed that, RFP-ARA7-
350 positive structures had an overlap with YFP-TTN5 (29 %) and even more with YFP-TTN5^{Q70L}
351 (75 %) unlike with YFP-TTN5^{T30N} (21 %) (Supplementary Figure S8D). Based on this, YFP-
352 TTN5^{Q70L} and YFP-TTN5 tended to colocalize better with ARA7-positive compartments than
353 YFP-TTN5^{T30N}.
354 To prove MVB localization, we treated plant cells with wortmannin, a common approach to
355 studying endocytosis events. Wortmannin is a fungal metabolite that inhibits
356 phosphatidylinositol-3-kinase (PI3K) function and thereby causes swelling of the MVBs (Cui et
357 al., 2016) (Figure 4M). RFP-ARA7-expressing cells showed the expected typical wortmannin-
358 induced formation of doughnut-like shaped MVBs (Jaillais et al., 2008). The coexpressed YFP-
359 TTN5 constructs partially colocalized with these structures (Figure 4N-P) proving YFP-TTN5
360 and the two mutants are present in MVBs. YFP-TTN5^{Q70L} was located even to a greater extent
361 to MVBs than wild-type YFP-TTN5 and much more than the YFP-TTN5^{T30N} mutant, suggesting
362 an active role of YFP-TTN5^{Q70L} in MVBs like the lytic degradation pathway or the recycling of
363 proteins, similar to ARA7 (Kotzer et al., 2004).
364 Finally, to investigate the connection of TTN5 with the plasma membrane, we colocalized
365 the YFP-TTN5 proteins with the dye FM4-64, which can emit fluorescence in a lipophilic
366 membrane environment and marks the plasma membrane in the first minutes following
367 application to the cell (Bolte et al., 2004) (Figure 5A). All three forms of TTN5 colocalized with
368 FM4-64 at the plasma membrane in a similar manner (Figure 5B-D). To further prove plasma
369 membrane localization, we performed mannitol-induced plasmolysis. All three YFP-TTN5
370 protein forms were located similarly to FM4-64-stained Hechtian strands, which are thread-like
371 structures attached to the apoplast visible upon plasmolysis that is lined by plasma membrane
372 (Figure 5E-G).

373 In summary, these colocalization experiments showed that YFP-TTN5 locates in different
374 membrane sites of the endomembrane system, including Golgi, MVBs, and plasma
375 membrane. We figured that similar to other ARF proteins, TTN5 might participate in a highly
376 dynamic vesicle trafficking process. Indeed, when we recorded the dynamic movement of YFP
377 signals inside *N. benthamiana* leaf epidermis cells, YFP-TTN5 and YFP-TTN5^{Q70L} colocalized
378 with GmMan1-mCherry and revealed high motion over time, while this was less the case for
379 YFP-TTN5^{T30N} (Supplementary Video Material S2A-C).
380 One potential cellular trafficking route is the degradation pathway to the vacuole. We,
381 therefore, investigated YFP-TTN5 localization in late endosomal compartments that might be
382 involved in vacuolar targeting. FM4-64 is used as a marker for vacuolar degradation targeting,
383 since following plasma membrane visualization FM4-64-stained endocytic vesicles become
384 apparent at later stages as well as vacuolar membrane staining (Ueda et al., 2001; Emans et
385 al., 2002; Dhonukshe et al., 2007; Ivanov and Vert, 2021). Hence, we colocalized YFP-TTN5
386 with FM4-64-positive compartments at later time points. Next to YFP-TTN5 colocalization with
387 FM4-64 at the plasma membrane, we detected colocalization with fluorescent compartments
388 in the cell, which was similar for the two mutant forms (Figure 5H-J). This indicates that YFP-
389 TTN5 may be involved in the vacuolar targeting of plasma membrane material, irrespective of
390 the mutations.
391 In summary, YFP-TTN5^{T30N} tended to be less mobile and dynamic and colocalized less with
392 endomembrane structures compared to YFP-TTN5 and YFP-TTN5^{Q70L}.

393 **Discussion**

394 This work showed that the small ARF-like GTPase TTN5 has a very rapid intrinsic nucleotide
395 exchange capacity with a conserved nucleotide switching mechanism. Enzyme kinetics
396 indicate that TTN5 might be primarily present in a GTP-loaded active form in a cell. YFP-TTN5
397 was dynamically associated with vesicle transport and different processes of the
398 endomembrane system. The active TTN5^{Q70L} mutant was capable of nucleotide switching, and
399 YFP-TTN5^{Q70L} had localization properties comparable with YFP-TTN5. The dominant negative
400 YFP-TTN5^{T30N} mutant, on the other hand, had a lower nucleotide exchange capacity than the
401 other TTN5 forms and it differed significantly in localization properties depending on cell types.
402 Therefore, this mutation affected the cellular localization and dynamics of TTN5.
403

404 **TTN5 exhibits characteristic GTPase functions**

405 TTN5 was classified as an ARL2 homolog of the ARF GTPases based on its sequence
406 similarity. The sequence analysis suggested nucleotide binding (McElver et al., 2000) which is
407 reinforced by structural prediction suggesting the formation of a nucleotide-binding pocket by
408 the binding motifs. Nucleotide association and dissociation of TTN5, TTN5^{T30N,} and TTN5^{Q70L}
409 proved that TTN5 along with the two mutant forms can bind guanine nucleotides. The k_{on} value
410 for TTN5^{Q70L}, which is described as a GTP hydrolysis-defective mutant (Dascher and Balch,
411 1994), was clearly higher than that of the wild-type form, indicating that this mutant can bind
412 GDP faster than TTN5 to form the nucleotide-bound form. Compared with other members of
413 the Ras superfamily, it was in the range of HRAS (Hanzal-Bayer et al., 2005) and around ten
414 times slower than the fast association of RAC1 (Jaiswal et al., 2013). The k_{on} values of
415 TTN5^{T30N} and TTN5 were nearly the same, indicating no effect of the mutation on the GDP-
416 binding characteristics as was expected in the absence of a GEF. Intrinsic nucleotide exchange
417 measurements of TTN5 and TTN5^{Q70L} have shown remarkably fast nucleotide exchange rates,
418 when compared to other well-studied RAS proteins. The intrinsic nucleotide exchange reaction
419 rates for RAC1, RAC2, and RAC3 have been mentioned around 40.000 s (Haeusler et al.,
420 2006). Our data show that TTN5 is faster in nucleotide exchange rate and very similar to that

421 of human homolog ARL2 (Hanzal-Bayer et al., 2005; Veltel et al., 2008). This explains that
422 TTN5 tends to quickly replace GDP for GTP and transforms from an inactive to an active state.
423 This behavior indicates that TTN5 does not require interaction with GEFs for activation. This
424 explanation seems also the case for TTN5^{Q70L}. Small GTPases with substitutions of the
425 glutamine of the switch II region (*e.g.*, Glu-71 for HsARF1 and ARL1, Glu-61 for HRAS) are
426 constitutively active (Zhang et al., 1994; Van Valkenburgh et al., 2001; Karnoub and Weinberg,
427 2008). Therefore, TTN5^{Q70L} is likely to exchange GDP rapidly to GTP and switch itself to stay
428 in an active form as suggested by the fast intrinsic nucleotide exchange rate. Interestingly,
429 dominant negative TTN5^{T30N} resulted in an even higher dissociation rate constant k_{off}. The
430 calculated K_d confirmed the higher nucleotide-binding affinity for GDP of TTN5 and TTN5^{Q70L}
431 compared with TTN5^{T30N}. Reports on human ARL2, ARF6, and ARL4D showed that their
432 corresponding T30N mutants led to a decreased affinity to GDP similar to TTN5^{T30N} (Macia et
433 al., 2004; Hanzal-Bayer et al., 2005; Li et al., 2012).
434 Interestingly, a comparison of mdGDP with mGppNHp revealed a higher GTP affinity for all
435 three versions, with the highest for TTN5^{Q70L}. These high GTP affinities in combination with the
436 fast GDP exchange rates and extremely slow hydrolysis pinpointed to a GTP-loaded TTN5
437 even in the rested state, which is very uncommon for small GTPases. This atypical behavior
438 is already reported for a few non-classical RHO GTPases like RHOD or RIF (Jaiswal et al.,
439 2013). This unusual GTP-bound active state along with the lacking N-myristoylation and
440 phylogenetic distances (Boisson et al., 2003; Vernoud et al., 2003) strengthens that there are
441 major differences between TTN5 and other ARF family members. The similarity between the
442 wild type and TTN5^{Q70L} is consistent with the previous report on human ARL2 in which wild-
443 type and Q70L proteins showed only a little difference in binding affinity (Hanzal-Bayer et al.,
444 2005). Additionally, an equivalent ratio of nucleotide affinity was found between HRAS and
445 HRAS^{Q61L}, but with a much higher affinity typical for small GTPases (Der et al., 1986). Since
446 Gln-70 at the switch II region is important for GAP-stimulated GTP hydrolysis (Cherfils and
447 Zeghouf, 2013), we assume that nucleotide exchange activity is unaffected by this amino acid
448 substitution.
449 To date, no GEF protein for TTN5 is reported. The Arabidopsis genome encodes only two
450 of the five mammalian GEF subgroups, namely the large ARF-GEF subgroups, the BFA-
451 inhibited GEF (BIG), and the Golgi Brefeldin A (BFA)-resistance factor 1 (GBF/GNOM) family
452 (Memon, 2004; Wright et al., 2014; Brandizzi, 2018). Potential interactions with these proteins
453 are of high interest and can also point to functions of TTN5 as a co-GEF as it is proposed for
454 HsARL3 and HsARL2 with their effector BART by stabilizing the active GTPase (ElMaghloob
455 et al., 2021). Especially, interactions at the nucleotide-binding site, which are prevented in the
456 TTN5^{T30N} mutant, will be of great interest to study further functions and interaction partners of
457 TTN5.
458 Taken together, the categorization as a non-classical GTPase has three implications:
459 First, the very slow hydrolysis rate predicts the existence of a TTN5 GAP. Second, TTN5^{T30N}
460 is a dominant negative mutant and in the presence of a GEF, it cannot bind GDP. Third, the
461 TTN5^{Q70L} hydrolysis rate is not decreased.

462 **YFP-TTN5 is part of the endomembrane system**

463 The ARF family of small GTPases is well known for its involvement in vesicle trafficking and
464 coat assembly with diverse localization patterns within the cell. We observed YFP-TTN5 to be
465 localized at different cellular compartments which is typical for several members of this family
466 and emphasizes its involvement in endomembrane trafficking (Memon, 2004; Sztul et al.,
467 2019). A detailed colocalization analysis showed that both *cis*-Golgi and MVB-positive
468 structures colocalized to a higher proportion with the YFP-TTN5^{Q70L} compared with YFP-

469 TTN5^{T30N}. This could be an indicator of the site of TTN5 action, considering our knowledge of
470 the activation of ARF GTPases and TTN5 homologs in other organisms. They are usually
471 recruited or move to their place of action upon interacting with their specific GEF, which leads
472 to GDP to GTP exchange-dependent activation (Sztul et al., 2019; Nielsen, 2020; Adarska et
473 al., 2021). Though our biochemical data implies no need for a typical GTPase-GEF interaction
474 for activation, GEF interaction can be still important for the localization. Most of the effector-
475 GTPase interactions take place in their GTP-bound form (Sharer and Kahn, 1999; Hanzal-
476 Bayer et al., 2005). One exception is the role of TTN5 homologs in microtubule dynamics.
477 ARL2/Alp41-GDP interacts with Cofactor D/Alp1^{D} (Bhamidipati et al., 2000; Mori and Toda,
478 2013). Another possibility is a hindrance of dimerization by the T30N mutation. ARF1 protein
479 dimer formation is important for the formation of free vesicles (Beck et al., 2009; Beck et al.,
480 2011) associated with cell mobility which was disturbed in YFP-TTN5^{T30N}-expressing cells. The
481 colocalization of YFP-TTN5 with ARA7-positive structures even still in the wortmannin-induced
482 swollen state, triggered by the homotypic fusion of MVBs (Wang et al., 2009), may indicate
483 that TTN5 performs similar functions in relation to ARA7. ARA7 is involved in cargo transport
484 in the endocytic pathway to the vacuole, with a role, for example, in the endocytosis of plasma
485 membrane material (Ueda et al., 2001; Sohn et al., 2003; Kotzer et al., 2004; Ebine et al.,
486 2011). Colocalization of YFP-TTN5 with FM4-64-labeled endocytosed vesicles leads to the
487 assumption of a TTN5 involvement in endocytosis and the degradation pathway to the vacuole.
488 Our colocalization data with the different markers reinforces the suggestion that TTN5 has
489 functions in vesicle trafficking.
490 A potential explanation of the localization to similar compartments of YFP-TTN5 and YFP-
491 TTN5^{Q70L} compared to inactive YFP-TTN5^{T30N} can be based on a special feature of TTN5 in
492 the ARF family. ARF GTPases are mostly myristoylated on Gly-2, which is essential for their
493 membrane binding. TTN5 as well as ARL2 and ARL3 lack this myristoylation though Gly-2 is
494 present (Boisson et al., 2003; Kahn et al., 2006). ARL2 and ARL3 are still able to bind
495 membranes, probably only by their N-terminal amphipathic helix as it was established for
496 SAR1, with an ARL2 membrane-binding efficiency being nucleotide-independent (Lee et al.,
497 2005; Kapoor et al., 2015). We suggest similar binding efficiency for TTN5 as all YFP-tagged
498 TTN5 forms localized to membranous compartments. But based on the varying colocalization
499 efficiency, with the YFP-TTN5^{T30N} signal being less prominent at the Golgi and MVBs,
500 compared to YFP-TTN5 and YFP-TTN5^{Q70L}, we hypothesize a nucleotide- or nucleotide
501 exchange-dependent specificity for different membranes with TTN5 in the resting state being
502 predominantly present close to the plasma membrane and being active in the endomembrane
503 system. Interestingly, with respect to the intracellular dynamics, we observed that the TTN5^{T30N}
504 mutant had a different behavior in different organ types. This might be due to differing GEFs
505 being differentially expressed. Likewise, it is conceivable that the constitutively expressed
506 TTN5 has different effector binding partners.
507 This broad diversity of biological functions of TTN5 homologs associated with different
508 signaling cascades is also reflected by very different protein partners for that. Few homologs
509 of human ARL2 interaction partners are present in Arabidopsis. It is therefore exceedingly
510 interesting to identify interacting proteins to determine whether TTN5 performs similar
511 functions as HsARL2 or what other role it may play. Such interactions might also explain why
512 TTN5 is essential in plants with regard to a potential GTP-dependence for TTN5 function which
513 fits to already known functions of other ARF GTPases (Sztul et al., 2019; Nielsen, 2020;
514 Adarska et al., 2021). In addition, ARF proteins are affected by a similar set of GEFs and
515 GAPs, indicating an interconnected network in ARF signaling. ARF double knockdowns
516 revealed specific phenotypes, suggesting redundancy in the ARF family (Volpicelli-Daley et

517 al., 2005; Kondo et al., 2012; Nakai et al., 2013; Adarska et al., 2021). The investigation of the
518 TTN5 connection in the ARF family might reveal a missing link in ARF signaling and cell traffic.
519 In our study, the pro35S::YFP-TTN5 and mutant forms did not complement the *ttn5-1*
520 mutant phenotype although there is constitutive expression of *TTN5*. There could be
521 differences in TTN5 levels in some cell types. Overexpression of ARF1 did not affect
522 intracellular localization compared to endogenous tagged-ARF1 but differed in function to form
523 tubulated structures (Bottanelli et al., 2017). Though constitutively driven, the YFP-TTN5
524 expression may be delayed or insufficient at the early embryonic stages resulting in the lack
525 of embryo-lethal complementation. On the other hand, the very fast nucleotide exchange
526 activity may be hindered by the presence of a large YFP-tag in comparison with the small HA_3-
527 tag which is able to rescue the embryo-lethality. This represents a potential limitation for the
528 localization of small GTPases with rapid nucleotide exchange in plants.
529
530 **Conclusion**
531 In this study, we identified TTN5 as a functional GTPase of the ARF-like family. TTN5 had
532 not only sequence similarity with human ARL2 but also the two proteins share a very rapid
533 nucleotide exchange capacity in contrast to other characterized ARF/ARL proteins. TTN5 has
534 a faster nucleotide dissociation rate to a slower GTP hydrolysis rate and a higher affinity to
535 GTP compared to GDP. Thus, TTN5 is a non-classical GTPase that most likely accumulate in
536 a GTP-bound state in cells. The nucleotide exchange capacity affected the localization and
537 dynamics of YFP-tagged TTN5 protein forms and associated TTN5 with the endomembrane
538 system. In the future, the identification of potential TTN5 GEF and GAP proteins as well as
539 other interaction partners and effector proteins will be of great interest to clarify the role of
540 TTN5 in endomembrane trafficking and cell-physiological responses.
541
542 **Material & Methods**

543 **Arabidopsis plant material and growth conditions**
544 The Arabidopsis *ttn5-1* mutant was previously described (McElver et al., 2000).
545 Heterozygous seedlings were selected by genotyping using the primers TTN5 intron1 fwd and
546 pDAP101 LB1 (Supplementary Table S1). For pro35S::YFP-TTN5 and pro35S::HA_3-TTN5
547 constructs, *TTN5*, $TTN5^{T30N,}$ and $TTN5^{Q70L}$ coding sequences were amplified with B1 and B2
548 attachment sites for Gateway cloning (Life Technologies) using the primer TITAN5 n-ter B1
549 and TITAN5 stop B2 (Supplementary Table S1). The obtained PCR fragments were cloned *via*
550 BP reaction (Life Technologies) into pDONR207 (Invitrogen). pro35S::YFP-TTN5 and
551 pro35S::HA_3-TTN5 constructs were created *via* LR reaction (Life Technologies) with the
552 destination vector pH7WGY2 (Karimi et al., 2005) and pALLIGATOR2 (Bensmihen et al.,
553 2004), respectively. Agrobacteria were transformed with obtained constructs and used for
554 stable Arabidopsis transformation (adapted by (Clough and Bent, 1998). Arabidopsis seeds
555 were sterilized with sodium hypochlorite solution (6 % Sodium hypochlorite and 0.1 % Triton
556 X-100) and stored for 24 hours at 4°C for stratification. Seedlings were grown upright on half-
557 strength Hoagland agar medium (1.5 mM $Ca(NO_3)_2$, 0.5 mM KH_2PO_4, 1.25 mM KNO_3,
558 0.75 mM $MgSO_4$, 1.5 µM $CuSO_4$, 50 µM H_3BO_3, 50 µM KCl, 10 µM $MnSO_4$, 0.075 µM
559 $(NH_4)_6Mo_7O_{24}$, 2 µM $ZnSO_4$, 50 µM FeNaEDTA and 1 % sucrose, pH 5.8, supplemented with
560 1.4 % Plant agar (Duchefa)] in growth chambers (CLF Plant Climatics) under long-day
561 condition (16 hours light at 21°C, 8 hours darkness at 19°C). Seedlings were grown for six
562 days (six-day system) or 17 days with the last three days on fresh plates (two-week system).
563 *Nicotiana benthamiana* plants were grown on soil for 2-4 weeks in a greenhouse facility
564 under long-day conditions (16 hours of light, 8 hours of darkness).

565
566 **Point mutant generation of *TTN5***
567 pDONR207:TTN5 was used as a template for site-directed *TTN5* mutagenesis. Primers
568 T5T30Nf and T5T30Nr (Supplementary Table S1) were used to amplify the entire vector
569 generating the $TTN5^{T30N}$ coding sequence and primers TQ70Lf and T5Q70Lr (Supplementary
570 Table S1) were used to amplify the entire vector generating the $TTN5^{Q70L}$ coding sequence.
571 The PCR amplifications were run using the following conditions: 95°C, 30 s; 18 cycles of 95°C,
572 30 s/ 55°C, 1 min/ 72°C 8 min; 72°C, 7 min. The completed reaction was treated with 10 units
573 of DpnI endonuclease for 1 h at 37°C and then used for *E. coli* transformation. Successful
574 mutagenesis was confirmed by Sanger sequencing.
575
576 ***In vitro* GTPase activity assays**
577 An overview of protein expression and purification is shown in Supplementary Figure S2A.
578 Recombinant pGEX-4T-1 bacterial protein expression vectors (Amersham, Germany)
579 containing coding sequences for *TTN5*, $TTN5^{T30N}$ and $TTN5^{Q70L}$ were transferred into *E. coli*
580 BL21 (DE3) Rosetta strain (Invitrogen, Germany). Following induction of GST-TTN5 fusion
581 protein expression according to standard procedures. Cell lysates were obtained after cell
582 disruption with a probe sonicator (Bandelin sonoplus ultrasonic homogenizer, Germany) using
583 a standard buffer (300 mM NaCl, 3 mM Dithiothreitol (DTT), 10 mM $MgCl_2$, 0.1 mM GDP, 1 %
584 Glycerol, and 50 mM Tris-HCl, pH 7.4). GST-fusion proteins were purified by loading total
585 bacterial lysate on a preequilibrated glutathione Sepharose column (Sigma, Germany) using
586 fast performance liquid chromatography system (Cytiva, Germany) (Step 1, affinity-purified
587 GST-TTN5 protein fraction). GST-tagged protein fractions were incubated with thrombin
588 (Sigma, Germany) at 4°C overnight for cleavage of the GST tag (Step 2, GST cleavage) and
589 applied again to the affinity column (Step 3, yielding TTN5 protein fraction). Purified proteins
590 were concentrated using 10 kDa ultra-centrifugal filter Amicon (Merck Millipore, Germany). The
591 quality and quantity of proteins were analyzed by SDS-protein gel electrophoresis (Bio-Rad),
592 UV/Vis spectrometer (Eppendorf, Germany), and high-performance liquid chromatography
593 (HPLC) using a reversed-phase C18 column (Sigma, Germany) and a pre-column (Nucleosil
594 100 C18, Bischoff Chromatography) as described (Eberth and Ahmadian, 2009)
595 (Supplementary Figure S2B-D).
596 Nucleotide-free TTN5 protein was prepared from the TTN5 protein fraction (Eberth and
597 Ahmadian, 2009) as illustrated in Supplementary Figure S2E. 0.5 mg TTN5 protein was
598 combined with 1 U of agarose bead-coupled alkaline phosphatase (Sigma Aldrich, Germany)
599 for degradation of bound GDP to GMP and Pi in the presence of 1.5-fold molar excess of non-
600 hydrolyzable GTP analog GppCp (Jena Bioscience, Germany). After confirmation of GDP
601 degradation by HPLC, 0.002 U snake venom phosphodiesterase (Sigma Aldrich, Germany)
602 per mg TTN5 was added to cleave GppCp to GMP, G, and Pi. The reaction progress of
603 degradation of nucleotides was analyzed by HPLC using 30 µM TTN5 in 30 µl injection volume
604 (Beckman Gold HPLC, Beckman Coulter). After completion of the reaction, in order to remove
605 the agarose bead–coupled alkaline phosphatase, the solution was centrifuged for 10 min at
606 10000 *g*, 4°C, which was followed by snap freezing and thawing cycles to inactivate the
607 phosphodiesterase. mdGDP (2-deoxy-3-O-N-methylanthraniloyl GDP)- and mGppNHp 2'/3'-
608 O-(N-Methyl-anthraniloyl)-guanosine-5'-[(β,γ)-imido]triphosphate)-bound TTN5, $TTN5^{T30N}$ and
609 $TTN5^{Q70L}$ were prepared by incubation of nucleotide-free forms with fluorescent nucleotides
610 (Jena Bioscience, Germany) in a molar ratio of 1 to 1.2. The solution was purified from excess
611 amount of mdGDP and mGppNHp by using prepacked gel-filtration NAP-5 Columns (Cytiva,

612 Germany) to remove unbound nucleotides. Protein and nucleotide concentration were
613 determined using the Bradford reagent (Sigma Aldrich, Germany) and HPLC, respectively.
614 All kinetic fluorescence measurements including nucleotide association and dissociation
615 reactions were monitored on a stopped-flow instrument system SF-61, HiTech Scientific (TgK
616 Scientific Limited, UK) and SX20 MV (Applied Photophysics, UK) at 25°C using nucleotide
617 exchange buffer (10 mM K_2HPO_4/KH_2PO_4, pH 7.4, 5 mM $MgCl_2$, 3 mM DTT, 30 mM Tris/HCl,
618 pH 7.5) (Eberth and Ahmadian, 2009). Fluorescence was detected at 366 nm excitation and
619 450 nm emission using 408 nm cut-off filter for mant-nucleotides (Hemsath and Ahmadian,
620 2005).
621 To determine the intrinsic nucleotide exchange rate, k_{off}, 0.2 µM mdGDP- and mGppNHp-
622 bound proteins were combined with a 200-fold molar excess of 40 µM non-fluorescent GDP in
623 two different set of experiments, respectively. The decay of the fluorescence intensity
624 representing mdGDP and mGppNHp dissociation and replacement by non-fluorescent
625 nucleotide were recorded over time (Supplementary Figure S2G). Moreover, to determine the
626 nucleotide association rate, k_{on}, of mdGDP and mGppNHp to the nucleotide-free GTPase,
627 0.2 µM fluorescent nucleotides were mixed with different concentrations of nucleotide-free
628 TTN5 variants. The increase in the fluorescent intensity was obtained by the conformational
629 change of fluorescent nucleotides after binding to the proteins (Supplementary Figure S2H).
630 The data provided by stopped-flow were applied to obtain the observed rate constants.
631 Dissociation rate constants or nucleotide exchange rates (k_{off} in s^{-1}) and pseudo-first-order rate
632 constants or observed rate constants (k_{obs} in s^{-1}) at the different concentrations of the protein
633 were obtained by non-linear curve fitting using Origin software (version 2021b). The slopes
634 obtained from plotting k_{obs} against respective concentrations of proteins were used as the
635 second-order association rate constants (k_{on} in $\mu M^{-1}s^{-1}$). The equilibrium constant of
636 dissociation (K_d in µM) was calculated from the ratio of k_{off}/k_{on}. In order to investigate the
637 intrinsic GTP-hydrolysis rate of TTN5 variants, the HPLC method is used as described (Eberth
638 and Ahmadian, 2009). As an accurate strategy, HPLC provides the nucleotide contents over
639 time. The GTPase reaction rates were determined by mixing 100 µM nucleotide-free GTPase
640 and 100 µM GTP at 25°C in a standard buffer without GDP. The GTP contents were measured
641 at different times and the data were fitted with Origin software to get the observed rate
642 constant.
643

644 ***Nicotiana benthamiana* leaf infiltration**

645 *N. benthamiana* leaf infiltration was performed with the Agrobacterium (*Agrobacterium*
646 *radiobacter*) strain C58 (GV3101) carrying the respective constructs for confocal microscopy.
647 Agrobacteria cultures were grown overnight at 28°C, centrifuged for 5 min at 4°C at 5000*g*,
648 resuspended in infiltration solution (5 % sucrose, a pinch of glucose, 0.01 % Silwet Gold,
649 150 µM Acetosyringone), and incubated for 1 hour at room temperature. Bacterial suspension
650 was set to an OD_{600}=0.4 and infiltrated into the abaxial side of *N. benthamiana* leaves.

651

652 **Subcellular localization of fluorescent protein fusions**

653 Cloning of YFP-tagged TTN5 constructs is described in the paragraph 'Arabidopsis plant
654 material and growth conditions'. Localization studies were carried out by laser-scanning
655 confocal microscopy (LSM 780, Zeiss) with a 40x C-Apochromat water immersion objective.
656 YFP constructs and Alexa Fluor 488 stainings were excited at 488 nm and detected at 491-
657 560 nm. mCherry or FM4-64 fluorescence was excited at 561 nm and detected at 570-633 nm.

658 Wortmannin (10 µM, Sigma-Aldrich), BFA (36 µM, Sigma-Aldrich) and plasma membrane
659 dye FM4-64 (165 µM, ThermoFisher Scientific) were infiltrated into *N. benthamiana* leaves.
660 FM4-64 was detected after five min incubation. Wortmannin and BFA were incubated for
661 25 min before checking the treatment effect. Plasmolysis was induced by incubating leaf discs
662 in 1 M mannitol solution for 15 min. Signal intensities were increased for better visibility.
663

664 **Whole-mount Immunostaining**

665 Whole-mount immunostaining by immunofluorescence was performed according to the
666 protocol described by (Pasternak et al., 2015). Briefly, Arabidopsis seedlings were grown in
667 the standard condition in Hoagland media for 4-6 days. Methanol was used to fix the seedlings.
668 The seedlings were transferred to a glass slide and resuspended in 1x microtubule-stabilizing
669 buffer (MTSB). Seedlings were digested with 2 % Driselase dissolved in 1x MTSB at 37°C for
670 40 mins. Following digestion, permeabilization step was performed by treating the seedlings
671 with permeabilization buffer (3 % IGEPAL C630, 10 % dimethylsulfoxide (DMSO) in 1× MTSB
672 buffer) at 37°C for 20 mins. Then blocking was performed with a buffer consisting of 5 % BSA
673 for 30 min at room temperature. They were incubated overnight with rabbit anti-HA antibody
674 (1: 200 dilution, Abcam ab9110) at 37°C for 2 hours. After two washes with 1x MTSB, seedlings
675 were incubated with Alexa Fluor 488-labeled secondary antibody (1:200 goat anti-rabbit IgG,
676 Invitrogen, A32731) for 2 hours at 37°C. After five steps of washing with 1x PBS, coverslips
677 were mounted on slides with the antifade reagent (Prolong glass Antifade Mountant with
678 NucBlue Stain, Invitrogen). Fluorescence microscopy was conducted as described in the
679 previous section.
680

681 **JACoP based colocalization analysis**

682 Colocalization analysis was carried out with the ImageJ (Schneider et al., 2012) Plugin Just
683 Another Colocalization Plugin (JACoP) (Bolte and Cordelières, 2006) and a comparison of
684 Pearson's and Overlap coefficients and Li's intensity correlation quotient (ICQ) was performed.
685 Object-based analysis was done for punctate structures, adapted by (Ivanov et al., 2014).
686 Colocalization for both channels was calculated based on the distance between geometrical
687 centers of signals and presented as percentage. Analysis was done in three replicates each
688 (n = 3).

689

690 **Structure prediction**

691 TTN5 structure prediction was performed by AlphaFold (Jumper et al., 2021). The molecular
692 graphic was edited with UCSF ChimeraX (1.2.5, (Goddard et al., 2018), developed by the
693 Resource for Biocomputing, Visualization, and Informatics at the University of California, San
694 Francisco, with support from the National Institutes of Health R01-GM129325 and the Office
695 of Cyber Infrastructure and Computational Biology, National Institute of Allergy and Infectious
696 Diseases.
697

698 ***In silico* tool for gene expression analysis**

699 RNA-seq data relies on published data and was visualized with the AtGenExpress eFP at
700 bar.utoronto.ca/eplant (Waese et al., 2017).
701

702 **Statistical analysis**

One-way ANOVA was used for statistical analysis and performed in OriginPro 2019. Fisher LSD was chosen as a post-hoc test with $p < 0.05$.

ACCESSION NUMBERS

Sequence data from this article can be found in the TAIR and GenBank data libraries under accession numbers: *ARA7* (TAIR: AT4G19640), *GmMan1* (Uniprot: Q0PKY2) and *TTN5* (TAIR: AT2G18390).

Acknowledgements

We thank Gintaute Matthäi and Elke Wieneke for their excellent technical assistance. We are thankful to Anna Sergeeva for advice and help with whole-mount immunolocalization. We thank Ksenia Trofimov for microscopy help and advice, and Natalie Köhler for experimental assistance. We are thankful for the assistance from Stefanie Weidtkamp-Peters and Sebastian Hänsch, members of the Center for Advanced Imaging (CAi) at Heinrich Heine University. RFP-ARA7 clones were a gift from Dr. Thierry Gaude.

This work was supported by the Deutsche Forschungsgemeinschaft (DFG, German Research Foundation) Project no. 267205415–SFB 1208, project B05 to P.B. and DFG AH 92/8-3 to A.M. and M.R.A.. Funding for instrumentation: Zeiss LSM780 + 4channel FLIM extension (Picoquant): DFG- INST 208/551-1 FUGG.

Figure legends

Figure 1: TTN5, a homolog of small ARF-like GTPases. (A), Sequence alignment of TTN5 with human HsARL2, Arabidopsis AtARF1, HsARF1, and HsHRAS created with Jalview (Waterhouse et al., 2009). The conserved G-motifs (G1-G5; indicated by red lines) are defined for the TTN5 and HRAS sequence. The secondary structure of TTN5 is depicted by red lines and corresponding cartoon (α-helix in green; β-sheet in orange). Conserved residues of TTN5 relevant in this work are highlighted by boxes: Gly-2, Thr-30 and Gln-70. (B), Model of the predicted GTPase nucleotide exchange and hydrolysis cycle of TTN5. TTN5 switches from an inactive GDP-loaded form to an active GTP-loaded one. GDP to GTP nucleotide exchange and GTP hydrolysis may be aided by a guanidine exchange factor (GEF) and a GTPase-activating protein (GAP). (C), Predicted protein structural model of TTN5; magenta, marks the GTP-binding pocket; N-terminal amphipathic helix is highlighted in orange; conserved Gly-2 in green; T30 and Q70, mutagenized in this study, shown in sticks. The model was generated with AlphaFold (Jumper et al., 2021), and adaptation was done with UCSF ChimeraX 1.2.5 (Goddard et al., 2018).

Figure 2: Biochemical properties of TTN5 proteins suggest that TTN5 is present in a GTP-loaded active form in cells. (A), Schematic illustration of the stopped-flow fluorescence device for monitoring the nucleotide-binding kinetics of the purified TTN5 protein heterologously expressed in bacteria (Supplementary Figure S2A-D). It consists of two motorized, thermostated syringes, a mixing chamber, and a fluorescence detector. Two different reagents 1 and 2 are rapidly mixed and transferred to a fluorescence detection cell within 4 ms. One of the reagents must contain a fluorescent reporter group. Here, mdGDP and mGppNHp were used to mimic GDP and GTP. (B), Schematic illustration of the nucleotide association. Nucleotide-free TTN5 (reagent 1; preparation see Supplementary Figure S2E) was rapidly mixed with mdGDP (reagent 2). A fluorescence increase is expected upon association of mdGDP with TTN5. Similar measurements are performed with mGppNHp instead of mdGDP. (C), Schematic illustration of the intrinsic nucleotide exchange. mdGDP-bound TTN5 (reagent 1) is mixed with a molar excess of GDP (reagent 2). A fluorescence

750 decrease is expected upon mdGDP dissociation from TTN5 and binding of free GDP. Similar
751 measurements are performed with mGppNHp. (D-E), Kinetics of association and dissociation
752 of fluorescent nucleotides with TTN5 proteins (WT, $TTN5^{T30N}$, $TTN5^{Q70L}$) are illustrated as bar
753 charts. The association of mdGDP (0.1 µM) or mGppNHp (0.1 µM) with increasing
754 concentration of $TTN5^{WT}$, $TTN5^{T30N}$, and $TTN5^{Q70L}$ was measured using a stopped-flow device
755 (see A, B; data see Supplementary Figure S3A-F, S4A-E). Association rate constants (k_{on} in
756 $\mu M^{-1}s^{-1}$) were determined from the plot of increasing observed rate constants (k_{obs} in s^{-1}) against
757 the corresponding concentrations of the TTN5 proteins. Intrinsic dissociation rates (k_{off} in s^{-1})
758 were determined by rapidly mixing 0.1 µM mdGDP-bound or mGppNHp-bound TTN5 proteins
759 with the excess amount of unlabeled GDP (see A, C, data see Supplementary Figure S3G-I,
760 S4F-H). The nucleotide affinity (dissociation constant or K_d in µM) of the corresponding TTN5
761 proteins was calculated by dividing k_{off} by k_{on}. When mixing mGppNHp with nucleotide-free
762 $TTN5^{T30N}$, no binding was observed (n.b.o.) under these experimental conditions. (F-G), GTP
763 hydrolysis of TTN5 proteins determined by HPLC. (F), Schematic illustration of the GTP
764 hydrolysis measurement. (G), GTP-bound TTN5 proteins (100 µM) were incubated at room
765 temperature at different time points before injecting them on a reversed-phase HPLC system.
766 Evaluated data (data see Supplementary Figure S5) resulted in the determination of the GTP
767 hydrolysis rates (k_{cat}) illustrated as bar charts. (H), TTN5 accumulated in a GTP-loaded active
768 form. GST-$TTN5^{WT}$ (46.5 kDa) was purified from bacterial cell lysates at three different volumes
769 in the presence of 0.1 µM unbound free GppNHp using glutathione beads. The nucleotide
770 contents and the protein purities were determined by HPLC and Coomassie Blue-stained SDS-
771 polyacrylamide gel electrophoresis. The presence of much higher amounts of GppNHp-bound
772 versus GDP-bound GST-TTN5 protein indicates that TTN5 rapidly exchanged bound
773 nucleotide und accumulated in this state.

774 **Figure 3: TTN5 was present in punctate structures.** Microscopic observations were made
775 in a plane underneath the plasma membrane at the cell peripheries. (A), Schematic
776 representation of an Arabidopsis seedling. Images were taken at three different positions of
777 the seedlings and imaged areas are indicated by a red rectangle. (B-J), YFP-TTN5, YFP-
778 $TTN5^{T30N}$ and YFP-$TTN5^{Q70L}$ protein localization in Arabidopsis seedlings *via* fluorescent
779 confocal microscopy. (B-D), YFP-TTN5 and its two mutant variants YFP-$TTN5^{T30N}$ and YFP-
780 $TTN5^{Q70L}$ were observed in stomata (indicated by empty white arrowhead) and in the epidermis
781 of cotyledons in punctate structures (indicated by filled white arrowhead). (E-G), Localization
782 in the hypocotyls showed the same pattern of punctate structures. (H-J), YFP-TTN5 and its
783 two mutant variants YFP-$TTN5^{T30N}$ and YFP-$TTN5^{Q70L}$ were present in punctate structures in
784 the root hair zone and in root hairs (indicated by filled magenta arrowhead). (K), Schematic
785 representation of a *N. benthamiana* plant, used for leaf infiltration for transient expression.
786 Imaged areas are indicated by a red rectangle. (L-N), YFP-TTN5 signals in *N. benthamiana*
787 leaf epidermal cells. YFP-TTN5 and its two mutant variants YFP-$TTN5^{T30N}$ and YFP-$TTN5^{Q70L}$
788 are present in punctate structures (indicated by white arrowheads) and in the nucleus
789 (indicated by empty magenta arrowheads). Scale bar 50 µm.

790 **Figure 4: YFP-TTN5 associated with the endomembrane system in *N. benthamiana* leaf**
791 **epidermal cells.** YFP-TTN5 and its variants YFP-$TTN5^{T30N}$ and YFP-$TTN5^{Q70L}$ were localized
792 in *N. benthamiana* leaf epidermal cells with specific markers *via* fluorescent confocal
793 microscopy. (A), Schematic representation of GmMan1 localization at the *cis*-Golgi site. (B-D),
794 Partial colocalization of YFP-TTN5 proteins with the Golgi marker GmMan1-mCherry at *cis*-
795 Golgi stacks (filled white arrowheads). Additionally, YFP-TTN5 constructs were expressed
796 individually in vesicular-like structures (empty white arrowheads). (E), Schematic
797 representation of GmMan1 localization at the ER after redistribution of the Golgi to the ER

798 upon brefeldin A (BFA) treatment. (F-H), Redistribution of Golgi stacks was induced by BFA
799 treatment. GmMan1-mCherry and YFP-TTN5 constructs were present in the ER and in
800 coexpressing punctate structures. (I), Schematic representation of ARA7 localization at the
801 *trans*-Golgi network (TGN) and multi-vesicular bodies (MVBs). (J-L), Colocalization of YFP-
802 TTN5 proteins with the MVB marker RFP-ARA7. (M), Schematic representation of ARA7
803 localization in swollen MVBs upon wortmannin treatment. (N-P), MVB swelling was obtained
804 by wortmannin treatment. ARA7-RFP was colocalizing with YFP-TTN5 constructs in these
805 swollen MVBs. Chemical treatment-induced changes were imaged after 25 min incubation.
806 Colocalization is indicated with filled arrowheads, YFP-tagged construct expression alone with
807 empty ones. Corresponding colocalization analysis data is presented in Supplementary Figure
808 S8. Scale bar 10 µm.

809 **Figure 5. YFP-TTN5 colocalized with endocytosed plasma membrane material.** (A),
810 Schematic representation of FM4-64 plasma membrane localization and endocytosis. (B-J),
811 YFP-tagged TTN5 and mutant forms YFP-TTN5^{T30N} andYFP-TTN5^{Q70L} were localized in
812 *N. benthamiana* leaf epidermal cells together with the plasma membrane dye FM4-64 *via*
813 fluorescent confocal microscopy. (B-D), YFP-TTN5, YFP-TTN5^{T30N} and YFP-TTN5^{Q70L}
814 colocalized with FM4-64 at the plasma membrane. (E-G), YFP-TTN5 protein plasma
815 membrane localization was tested by mannitol-induced (1 M) plasmolysis. The formation of
816 Hechtian strands is indicated with filled arrowheads. (H-J), Internalized FM4-64 was present
817 in YFP-TTN5 and the respective GTPase-variant coexpressing vesicle-like structures.
818 Colocalization is indicated with filled arrowheads. Scale bar 10 µm.

819 **Supplementary Figure S1. *TTN5* gene expression based on transcriptome data.**
820 Ubiquitous expression of *TTN5* in (A), aerial organs of different developmental stages, (B), of
821 seedling root tissues based on single cell analysis, and (C), in successive stages of embryo
822 development. Data was visualized with AtGenExpress eFB tool (bar.utoronto.ca/eplant,
823 (Waese et al., 2017).

824 **Supplementary Figure S2. Heterologous expression and purification of TTN5 protein as**
825 **well as preparation of its nucleotide-free form.** (A), Overview of protein purification and
826 preparation of nucleotide-free form of TTN5 in the presence of excess GDP. (B-C), The
827 chromatograms represent the GST-affinity chromatography to obtain GST-TTN5 and TTN5
828 variants, before and after GST-cleavage by thrombin. (D), Coomassie Blue SDS-PAGE of
829 GST-TTN5 (left panel; 46.5 kDa) and TTN5 after GST-cleavage by thrombin and a second
830 GST-affinity chromatography (right panel; 21 kDa). (E), Schematic illustration of nucleotide-
831 free TTN5 preparation. In the first step, the purified GDP-bound TTN5 is incubated with alkaline
832 phosphatase in the presence of 1.5-fold molar excess of Gpp(CH_2)p, which is a non-
833 hydrolyzable GTP analog and, unlike GDP, resistant to alkaline phosphatase. After GDP is
834 completely degraded, phosphodiesterase is added to the reaction to degrade Gpp(CH_2)p to
835 GMP, G and Pi. The nucleotide content is monitored in each step by HPLC. The solution with
836 nucleotide-free TTN5 is deep-frozen and thawed twice, aliquoted and stored at -80°C.

837 **Supplementary Figure S3. Kinetic measurements of mdGDP interaction with TTN5**
838 **proteins.** (A-C), Association of mdGDP (0.1 µM) with increasing concentrations of TTN5^{WT}
839 (A), TTN5^{T30N} (B) and TTN5^{Q70L} (C). (D-F), Association rate constant (k_{on}) is determined by
840 plotting the k_{obs} values, obtained from the exponential fits of the mdGDP association data (A-
841 C) against the TTN5 (D), TTN5^{T30N} (E) and TTN5^{Q70L} (F) protein concentrations. (G-I),
842 Dissociation of mdGDP from TTN5 (G), TTN5^{T30N} (H) and TTN5^{Q70L} (I) proteins (0.1 µM) is
843 determined in the presence of excess amounts of unlabeled GDP (20 µM). The dissociation
844 rates (k_{off}) are obtained from the exponential fitting of the data by Origin software. All results

845 are shown as bar charts in Figure 2D. The principles of the assays are illustrated in Figure 2A-
846 C.

847 **Supplementary Figure S4. Kinetic measurements of mGppNHp interaction with TTN5**
848 **proteins.** (A-E), Association kinetics. (A, C), Association of mGppNHp (0.1 μM) with increasing
849 concentrations of $TTN5^{WT}$ (A) and $TTN5^{Q70L}$ (C). (B) When mixing mGppNHp with nucleotide-
850 free $TTN5^{T30N}$, no binding was observed under these experimental conditions. Instead,
851 association of mGppNHp (0.1 μM) with two different titrations of 0.5 μM $TTN5^{T30N}$ was
852 measured, indicated by arrows, to confirm the fast binding of $TTN5^{T30N}$ with mGppNHp by
853 increasing fluorescence intensity, determined by fluorimeter. (D-E), Association rate constant
854 (k_{on}) is determined by plotting the k_{obs} values, obtained from the exponential fits of the
855 mGppNHp association data (left panels) against the $TTN5^{WT}$ (D), and $TTN5^{Q70L}$ (E) protein
856 concentrations. Note that $TTN5^{T30N}$ did not show association with mGppNHp, therefore middle
857 space is left empty. (F-H), Dissociation of mGppNHp from $TTN5^{WT}$ (F), $TTN5^{T30N}$ (G) and
858 $TTN5^{Q70L}$ (H) proteins (0.1 μM) is determined in the presence of excess amounts of unlabeled
859 GppNHp (20 μM). The dissociation rates (k_{off}) are obtained from the exponential fitting of the
860 data by Origin software. All results are shown as bar charts in Figure 2E. The principles of the
861 assays are illustrated in Figure 2A-C.

862 **Supplementary Figure S5. GTP hydrolysis reaction rates of the TTN5 proteins.** (A-C),
863 The GTP hydrolysis reaction rates (k_{cat}) of $TTN5^{WT}$ (A), $TTN5^{T30N}$ (B) and $TTN5^{Q70L}$ (C) proteins
864 (100 μM) were measured at 25°C. Aliquots of the reaction mixture at the indicated time points
865 were analyzed by HPLC as described in Materials and Methods. The obtained results are
866 shown as bar charts in Figure 2G. The principle of the assay is illustrated in Figure 2F.

867 **Supplementary Figure S6. YFP-TTN5 localization in Arabidopsis seedlings.** Microscopic
868 observations were made in a plane across the centers of most cells. (A), Schematic
869 representation of an Arabidopsis seedling. Images were taken at four different positions of the
870 seedlings and imaged areas are indicated by a red rectangle. (B-M), YFP-TTN5 signals in
871 Arabidopsis seedlings *via* fluorescent confocal microscopy. (B–D), YFP protein localization
872 was observed in the epidermis of cotyledons. YFP-TTN5 and its two mutant variants YFP-
873 $TTN5^{T30N}$ and YFP-$TTN5^{Q70L}$ were present in nucleus (indicated by empty white arrowhead)
874 and cytoplasm and at or in close proximity to the plasma membrane (indicated by filled white
875 arrowhead) in the epidermis of cotyledons. (E-G), localization in the hypocotyls showed clear
876 presence in the cytoplasm (indicated by empty magenta arrowhead), next to nuclear and
877 plasma membrane-related localization. (H-J), YFP-TTN5 and its two mutant variants YFP-
878 $TTN5^{T30N}$ and YFP-$TTN5^{Q70L}$ were present in nuclei, cytoplasm, at or close to the plasma
879 membrane in the root hair zone and in root hairs (indicated by filled magenta arrowhead) with
880 clear cytoplasmic localization. (K-M), localization at the root tip showed clear expression in
881 nuclei and cytoplasm, visible due to the smaller size of the vacuoles. (N), schematic
882 representation of a *N. benthamiana* plant, used for leaf infiltration for transient expression.
883 Imaged areas are indicated by a red rectangle. (O-Q), YFP-TTN5 signals in *N. benthamiana*
884 leaf epidermal cells *via* fluorescent confocal microscopy. YFP-TTN5 and its two mutant
885 variants YFP-$TTN5^{T30N}$ and YFP-$TTN5^{Q70L}$ were present in nucleus and cytoplasm and at or in
886 close proximity to the plasma membrane. Scale bar 50 μm.

887 **Supplementary Figure S7. Phenotypes of *ttn5-1* T-DNA insertion line and whole-mount**
888 **immunolocalization.** (A), Schematic representation of the *TTN5* exon-intron structure and T-
889 DNA insertion in the *ttn5-1* allele. The numbers below the exon numbers indicate base pairs
890 (bp). (B), Early embryo arrest phenotype of a homozygous *ttn5-1*$^{-/-}$ seed on the left in
891 comparison with a wild type (WT) seed of the same silique on the right; arrowheads, indicate

892 enlarged nuclei in the arrested embryo (filled) and endosperm (empty). Early embryo arrest
893 phenotypes were previously shown by (Mayer et al., 1999; McElver et al., 2000). Scale bar
894 1 cm. (C), Siliques of heterozygous *ttn5-1*$^{+/-}$ plants, containing ca. 25 % white seeds with
895 arrested embryos (filled arrowheads) and ca. 75 % regular green seeds (empty arrowheads).
896 HA_3-TTN5 line crossed to *ttn5-1*$^{+/-}$ was able to rescue embryo lethal seed phenotype. (D),
897 Whole-mount immunostaining of HA_3-TTN5 seedlings. HA_3-tagged TTN5 localization was
898 detected by α-HA/Alexa 488 immunostaining. HA_3-TTN5 was present in vesicle-like structures
899 in the root cells (indicated by filled white arrowhead) and in root hairs (indicated by filled
900 magenta arrowhead) comparable to YFP-TTN5 (Figure 3). Images are presented in a
901 maximum intensity projection of several z-layers for a better visualization. Scale bar 50 µm.

902 **Supplementary Figure S8. YFP-TTN5 is colocalized with GmMan1-mCherry and mRFP-**
903 **ARA7.** Colocalization analyses of the three YFP-TTN5 variants with specific markers using
904 ImageJ (Schneider et al., 2012). (A), JACoP-based colocalization analysis (Bolte and
905 Cordelières, 2006). Comparison of Pearson's and Overlap coefficients for *cis*-Golgi located
906 GmMan1-mCherry with the three YFP-TTN5 variants in vesicle-like structures was done. All
907 YFP-TTN5 variants colocalized similarly with the *cis*-Golgi marker. (B), Object-based analysis
908 was performed for vesicle-like structures based on distance between geometrical centers of
909 signals. YFP-TTN5-positive structures overlapped most with GmMan1-mCherry-positive Golgi
910 stacks, compared to YFP-TTN5^{T30N} and YFP-TTN5^{Q70L}. GmMan1-mCherry-positive Golgi
911 stacks overlap most with YFP-TTN5^{Q70L}-positive structures followed by YFP-TTN5 and YFP-
912 TTN5^{T30N}. (C), JACoP-based colocalization analysis (Bolte and Cordelières, 2006).
913 Comparison of Pearson's and Overlap coefficients for TGN/MVB located mRFP-ARA7 with the
914 three YFP-TTN5 variants in vesicle-like structures was done. YFP-TTN5 and YFP-TTN5^{Q70L}
915 colocalized similarly with the mRFP-ARA7, whereas YFP-TTN5^{T30N} tended to colocalize less.
916 (D), Object-based analysis was performed for vesicle-like structures based on distance
917 between geometrical centers of signals. More than half of all YFP-TTN5 variants-positive
918 structures overlapped with mRFP-ARA7-positive structures, in the order YFP-TTN5^{T30N}, YFP-
919 TTN5 and best YFP-TTN5^{Q70L}. mRFP-ARA7-positive structures overlapped most with YFP-
920 TTN5^{Q70L} and for YFP-TTN5 and YFP-TTN5^{T30N} being reduced by ca. 3.5-fold and 2.5-fold,
921 respectively. Analyses were conducted in three replicates each (n=3). One-way ANOVA with
922 Fisher-LSD post-hoc test was performed. Different letters indicate statistical significance ($p <$
923 0.05).

924 **Supplementary Video Material S1. YFP-TTN5 is present in dynamic vesicle-like**
925 **structures.** (A-O), Time series of YFP-TTN5, YFP-TTN5^{T30N} and YFP-TTN5^{Q70L} dynamic
926 expression in vesicle-like structures in Arabidopsis seedlings (A-L), or *N. benthamiana* leaf
927 epidermal cells (M-O) *via* fluorescence confocal microscopy. (A-C), YFP-TTN5 and its two
928 mutant variants YFP-TTN5^{T30N} and YFP-TTN5^{Q70L} were present in dynamic vesicle-like
929 structures in epidermal cotyledon cells and stomata. (D-F), Mobility in the hypocotyls of YFP-
930 TTN5^{T30N} (E) differed by a slower or aborted motion in half of the cells compared to YFP-TTN5
931 (D) and YFP-TTN5^{Q70L} (F). (G-I), YFP-TTN5 and its two mutant variants YFP-TTN5^{T30N} and
932 YFP-TTN5^{Q70L} were present in the same dynamic vesicle-like structures in the root hair zone
933 and in root hairs as well. (J-L), No clear mobility or vesicle-like structures were observed in the
934 root tips of YFP-TTN5, YFP-TTN5^{T30N} or YFP-TTN5^{Q70L} seedlings. (M-O), YFP-TTN5, YFP-
935 TTN5^{T30N} and YFP-TTN5^{Q70L} were present in dynamic vesicle-like structures in *N. benthamiana*
936 epidermal cells in a comparable manner to Arabidopsis seedlings. Scale bar 50 µm.

937

938 **References**

939 **Adarska P, Wong-Dilworth L, Bottanelli F** (2021) ARF GTPases and Their Ubiquitous Role
940 in Intracellular Trafficking Beyond the Golgi. Frontiers in cell and developmental biology
941 **9:** 679046-679046
942 **Ahmadi Y, Ghorbanihaghjo A, Argani H** (2017) The balance between induction and
943 inhibition of mevalonate pathway regulates cancer suppression by statins: A review of
944 molecular mechanisms. Chem Biol Interact **273:** 273-285
945 **Antoshechkin I, Han M** (2002) The *C. elegans* evl-20 Gene Is a Homolog of the Small
946 GTPase ARL2 and Regulates Cytoskeleton Dynamics during Cytokinesis and
947 Morphogenesis. Developmental Cell **2:** 579-591
948 **Beck R, Adolf F, Weimer C, Bruegger B, Wieland FT** (2009) ArfGAP1 Activity and COPI
949 Vesicle Biogenesis. Traffic **10:** 307-315
950 **Beck R, Prinz S, Diestelkötter-Bachert P, Röhling S, Adolf F, Hoehner K, Welsch S,**
951 **Ronchi P, Brügger B, Briggs JAG, Wieland F** (2011) Coatomer and dimeric ADP
952 ribosylation factor 1 promote distinct steps in membrane scission. The Journal of cell
953 biology **194:** 765-777
954 **Bensmihen S, To A, Lambert G, Kroj T, Giraudat J, Parcy F** (2004) Analysis of an activated
955 ABI5 allele using a new selection method for transgenic Arabidopsis seeds. FEBS Lett
956 **561:** 127-131
957 **Bhamidipati A, Lewis SA, Cowan NJ** (2000) ADP ribosylation factor-like protein 2 (Arl2)
958 regulates the interaction of tubulin-folding cofactor D with native tubulin. Journal of Cell
959 Biology **149:** 1087-1096
960 **Boisson B, Giglione C, Meinnel T** (2003) Unexpected Protein Families Including Cell
961 Defense Components Feature in the N-Myristoylome of a Higher Eukaryote*. Journal
962 of Biological Chemistry **278:** 43418-43429
963 **Bolte S, Cordelières FP** (2006) A guided tour into subcellular colocalization analysis in light
964 microscopy. J Microsc **224:** 213-232
965 **Bolte S, Talbot C, Boutte Y, Catrice O, Read ND, Satiat-Jeunemaitre B** (2004) FM-dyes as
966 experimental probes for dissecting vesicle trafficking in living plant cells. Journal of
967 Microscopy **214:** 159-173
968 **Bos JL** (1988) The ras gene family and human carcinogenesis. Mutation Research/Reviews
969 in Genetic Toxicology **195:** 255-271
970 **Bottanelli F, Kilian N, Ernst AM, Rivera-Molina F, Schroeder LK, Kromann EB, Lessard**
971 **MD, Erdmann RS, Schepartz A, Baddeley D, Bewersdorf J, Toomre D, Rothman**
972 **JE** (2017) A novel physiological role for ARF1 in the formation of bidirectional tubules
973 from the Golgi. Mol Biol Cell **28:** 1676-1687
974 **Brandizzi F** (2018) Transport from the endoplasmic reticulum to the Golgi in plants: Where
975 are we now? Semin Cell Dev Biol **80:** 94-105
976 **Brandizzi F, Snapp EL, Roberts AG, Lippincott-Schwartz J, Hawes C** (2002) Membrane
977 Protein Transport between the Endoplasmic Reticulum and the Golgi in Tobacco
978 Leaves Is Energy Dependent but Cytoskeleton Independent : Evidence from Selective
979 Photobleaching. The Plant Cell **14:** 1293-1309
980 **Brumm S, Singh MK, Nielsen ME, Richter S, Beckmann H, Stierhof YD, Fischer AM,**
981 **Kumaran M, Sundaresan V, Jürgens G** (2020) Coordinated Activation of ARF1
982 GTPases by ARF-GEF GNOM Dimers Is Essential for Vesicle Trafficking in
983 Arabidopsis. Plant Cell **32:** 2491-2507
984 **Cherfils J, Zeghouf M** (2013) Regulation of small GTPases by GEFs, GAPs, and GDIs.
985 Physiol Rev **93:** 269-309

986 **Clough SJ, Bent AF** (1998) Floral dip: a simplified method for Agrobacterium-mediated
987 transformation of Arabidopsis thaliana. Plant J **16:** 735-743
988 **Cui Y, Shen J, Gao C, Zhuang X, Wang J, Jiang L** (2016) Biogenesis of Plant Prevacuolar
989 Multivesicular Bodies. Molecular Plant **9:** 774-786
990 **Dascher C, Balch WE** (1994) Dominant inhibitory mutants of ARF1 block endoplasmic
991 reticulum to Golgi transport and trigger disassembly of the Golgi apparatus. J Biol
992 Chem **269:** 1437-1448
993 **Der CJ, Finkel T, Cooper GM** (1986) Biological and biochemical properties of human rasH
994 genes mutated at codon 61. Cell **44:** 167-176
995 **Dhonukshe P, Aniento F, Hwang I, Robinson DG, Mravec J, Stierhof Y-D, Friml J** (2007)
996 Clathrin-Mediated Constitutive Endocytosis of PIN Auxin Efflux Carriers in Arabidopsis.
997 Current Biology **17:** 520-527
998 **Eberth A, Ahmadian MR** (2009) In Vitro GEF and GAP Assays. Current Protocols in Cell
999 Biology **43:** 14.19.11-14.19.25
1000 **Ebine K, Fujimoto M, Okatani Y, Nishiyama T, Goh T, Ito E, Dainobu T, Nishitani A,**
1001 **Uemura T, Sato MH, Thordal-Christensen H, Tsutsumi N, Nakano A, Ueda T** (2011)
1002 A membrane trafficking pathway regulated by the plant-specific RAB GTPase ARA6.
1003 Nat Cell Biol **13:** 853-859
1004 **ElMaghloob Y, Sot B, McIlwraith MJ, Garcia E, Yelland T, Ismail S** (2021) ARL3 activation
1005 requires the co-GEF BART and effector-mediated turnover. Elife **10**
1006 **Emans N, Zimmermann S, Fischer R** (2002) Uptake of a fluorescent marker in plant cells is
1007 sensitive to brefeldin A and wortmannin. Plant Cell **14:** 71-86
1008 **Esposito A, Ventura V, Petoukhov MV, Rai A, Svergun DI, Vanoni MA** (2019) Human
1009 MICAL1: Activation by the small GTPase Rab8 and small-angle X-ray scattering
1010 studies on the oligomerization state of MICAL1 and its complex with Rab8. Protein Sci
1011 **28:** 150-166
1012 **Fansa EK, Wittinghofer A** (2016) Sorting of lipidated cargo by the Arl2/Arl3 system. Small
1013 GTPases **7:** 222-230
1014 **Fasano G, Muto V, Radio FC, Venditti M, Mosaddeghzadeh N, Coppola S, Paradisi G,**
1015 **Zara E, Bazgir F, Ziegler A, Chillemi G, Bertuccini L, Tinari A, Vetro A, Pantaleoni**
1016 **F, Pizzi S, Conti LA, Petrini S, Bruselles A, Prandi IG, Mancini C, Chandramouli**
1017 **B, Barth M, Bris C, Milani D, Selicorni A, Macchiaiolo M, Gonfiantini MV, Bartuli**
1018 **A, Mariani R, Curry CJ, Guerrini R, Slavotinek A, Iascone M, Dallapiccola B,**
1019 **Ahmadian MR, Lauri A, Tartaglia M** (2022) Dominant ARF3 variants disrupt Golgi
1020 integrity and cause a neurodevelopmental disorder recapitulated in zebrafish. Nat
1021 Commun **13:** 6841
1022 **Fisher S, Kuna D, Caspary T, Kahn RA, Sztul E** (2020) ARF family GTPases with links to
1023 cilia. American Journal of Physiology-Cell Physiology **319:** C404-C418
1024 **Fleming JA, Vega LR, Solomon F** (2000) Function of tubulin binding proteins in vivo.
1025 Genetics **156:** 69-80
1026 **Gimenez MC, Frontini-Lopez YR, Pocognoni CA, Roldán JS, Samartino CG, Uhart M,**
1027 **Colombo MI, Terebiznik MR, Delgui LR** (2022) Rab1b-GBF1-ARF1 Secretory
1028 Pathway Axis Is Required for Birnavirus Replication. Journal of Virology **96:** e02005-
1029 02021
1030 **Goddard TD, Huang CC, Meng EC, Pettersen EF, Couch GS, Morris JH, Ferrin TE** (2018)
1031 UCSF ChimeraX: Meeting modern challenges in visualization and analysis. Protein Sci
1032 **27:** 14-25

1033 **Gremer L, Merbitz-Zahradnik T, Dvorsky R, Cirstea IC, Kratz CP, Zenker M, Wittinghofer**
1034 **A, Ahmadian MR** (2011) Germline KRAS mutations cause aberrant biochemical and
1035 physical properties leading to developmental disorders. Hum Mutat **32:** 33-43
1036 **Haeusler LC, Hemsath L, Fiegen D, Blumenstein L, Herbrand U, Stege P, Dvorsky R,**
1037 **Ahmadian MR** (2006) Purification and biochemical properties of Rac1, 2, 3 and the
1038 splice variant Rac1b. Methods Enzymol **406:** 1-11
1039 **Hall A** (1990) The cellular functions of small GTP-binding proteins. Science **249:** 635-640
1040 **Hanton SL, Matheson LA, Chatre L, Brandizzi F** (2009) Dynamic organization of COPII coat
1041 proteins at endoplasmic reticulum export sites in plant cells. The Plant Journal **57:** 963-
1042 974
1043 **Hanzal-Bayer M, Linari M, Wittinghofer A** (2005) Properties of the interaction of Arf-like
1044 protein 2 with PDEdelta. J Mol Biol **350:** 1074-1082
1045 **Hemsath L, Ahmadian MR** (2005) Fluorescence approaches for monitoring interactions of
1046 Rho GTPases with nucleotides, regulators, and effectors. Methods **37:** 173-182
1047 **Heucken N, Ivanov R** (2018) The retromer, sorting nexins and the plant endomembrane
1048 protein trafficking. J Cell Sci **131**
1049 **Hillig RC, Hanzal-Bayer M, Linari M, Becker J, Wittinghofer A, Renault L** (2000) Structural
1050 and biochemical properties show ARL3-GDP as a distinct GTP binding protein.
1051 Structure **8:** 1239-1245
1052 **Ismail SA, Chen YX, Rusinova A, Chandra A, Bierbaum M, Gremer L, Triola G, Waldmann**
1053 **H, Bastiaens PI, Wittinghofer A** (2011) Arl2-GTP and Arl3-GTP regulate a GDI-like
1054 transport system for farnesylated cargo. Nat Chem Biol **7:** 942-949
1055 **Ito E, Uemura T, Ueda T, Nakano A** (2016) Distribution of RAB5-positive multivesicular
1056 endosomes and the trans-Golgi network in root meristematic cells of *Arabidopsis*
1057 *thaliana*. Plant biotechnology (Tokyo, Japan) **33:** 281-286
1058 **Ivanov R, Brumbarova T, Blum A, Jantke A-M, Fink-Straube C, Bauer P** (2014) SORTING
1059 NEXIN1 is required for modulating the trafficking and stability of the Arabidopsis IRON-
1060 REGULATED TRANSPORTER1. The Plant cell **26:** 1294-1307
1061 **Ivanov R, Vert G** (2021) Endocytosis in plants: Peculiarities and roles in the regulated
1062 trafficking of plant metal transporters. Biology of the Cell **113:** 1-13
1063 **Jaillais Y, Fobis-Loisy I, Miège C, Gaude T** (2008) Evidence for a sorting endosome in
1064 Arabidopsis root cells. The Plant Journal **53:** 237-247
1065 **Jaiswal M, Fansa EK, Dvorsky R, Ahmadian MR** (2013) New insight into the molecular
1066 switch mechanism of human Rho family proteins: shifting a paradigm. Biol Chem **394:**
1067 89-95
1068 **Jian X, Gruschus JM, Sztul E, Randazzo PA** (2012) The pleckstrin homology (PH) domain
1069 of the Arf exchange factor Brag2 is an allosteric binding site. J Biol Chem **287:** 24273-
1070 24283
1071 **Jumper J, Evans R, Pritzel A, Green T, Figurnov M, Ronneberger O, Tunyasuvunakool**
1072 **K, Bates R, Žídek A, Potapenko A, Bridgland A, Meyer C, Kohl SAA, Ballard AJ,**
1073 **Cowie A, Romera-Paredes B, Nikolov S, Jain R, Adler J, Back T, Petersen S,**
1074 **Reiman D, Clancy E, Zielinski M, Steinegger M, Pacholska M, Berghammer T,**
1075 **Bodenstein S, Silver D, Vinyals O, Senior AW, Kavukcuoglu K, Kohli P, Hassabis**
1076 **D** (2021) Highly accurate protein structure prediction with AlphaFold. Nature **596:** 583-
1077 589
1078 **Just WW, Peränen J** (2016) Small GTPases in peroxisome dynamics. Biochimica et
1079 Biophysica Acta (BBA) - Molecular Cell Research **1863:** 1006-1013

1080 **Kahn RA, Cherfils J, Elias M, Lovering RC, Munro S, Schurmann A** (2006) Nomenclature
1081 for the human Arf family of GTP-binding proteins: ARF, ARL, and SAR proteins. The
1082 Journal of cell biology **172:** 645-650
1083 **Kahn RA, Der CJ, Bokoch GM** (1992) The ras superfamily of GTP-binding proteins:
1084 guidelines on nomenclature. The FASEB Journal **6:** 2512-2513
1085 **Kapoor S, Fansa EK, Möbitz S, Ismail SA, Winter R, Wittinghofer A, Weise K** (2015) Effect
1086 of the N-Terminal Helix and Nucleotide Loading on the Membrane and Effector Binding
1087 of Arl2/3. Biophys J **109:** 1619-1629
1088 **Karimi M, De Meyer B, Hilson P** (2005) Modular cloning in plant cells. Trends in Plant Science
1089 **10:** 103-105
1090 **Karnoub AE, Weinberg RA** (2008) Ras oncogenes: split personalities. Nat Rev Mol Cell Biol
1091 **9:** 517-531
1092 **Kondo Y, Hanai A, Nakai W, Katoh Y, Nakayama K, Shin HW** (2012) ARF1 and ARF3 are
1093 required for the integrity of recycling endosomes and the recycling pathway. Cell Struct
1094 Funct **37:** 141-154
1095 **Kotzer AM, Brandizzi F, Neumann U, Paris N, Moore I, Hawes C** (2004) AtRabF2b (Ara7)
1096 acts on the vacuolar trafficking pathway in tobacco leaf epidermal cells. Journal of Cell
1097 Science **117:** 6377-6389
1098 **Latijnhouwers M, Hawes C, Carvalho C, Oparka K, Gillingham AK, Boevink P** (2005) An
1099 Arabidopsis GRIP domain protein locates to the trans-Golgi and binds the small
1100 GTPase ARL1. The Plant Journal **44:** 459-470
1101 **Lee GJ, Sohn EJ, Lee MH, Hwang I** (2004) The Arabidopsis rab5 homologs rha1 and ara7
1102 localize to the prevacuolar compartment. Plant Cell Physiol **45:** 1211-1220
1103 **Lee MC, Orci L, Hamamoto S, Futai E, Ravazzola M, Schekman R** (2005) Sar1p N-terminal
1104 helix initiates membrane curvature and completes the fission of a COPII vesicle. Cell
1105 **122:** 605-617
1106 **Li C-C, Wu T-S, Huang C-F, Jang L-T, Liu Y-T, You S-T, Liou G-G, Lee F-JS** (2012) GTP-
1107 Binding-Defective ARL4D Alters Mitochondrial Morphology and Membrane Potential.
1108 PLOS ONE **7:** e43552
1109 **Lloyd J, Meinke D** (2012) A comprehensive dataset of genes with a loss-of-function mutant
1110 phenotype in Arabidopsis. Plant Physiol **158:** 1115-1129
1111 **Macia E, Luton F, Partisani M, Cherfils J, Chardin P, Franco M** (2004) The GDP-bound
1112 form of Arf6 is located at the plasma membrane. J Cell Sci **117:** 2389-2398
1113 **Mayer U, Herzog U, Berger F, Inzé D, Jürgens G** (1999) Mutations in the PILZ group genes
1114 disrupt the microtubule cytoskeleton and uncouple cell cycle progression from cell
1115 division in Arabidopsis embryo and endosperm. European Journal of Cell Biology **78:**
1116 100-108
1117 **McElver J, Patton D, Rumbaugh M, Liu C-m, Yang LJ, Meinke D** (2000) The TITAN5 Gene
1118 of Arabidopsis Encodes a Protein Related to the ADP Ribosylation Factor Family of
1119 GTP Binding Proteins. The Plant Cell **12:** 1379-1392
1120 **Memon AR** (2004) The role of ADP-ribosylation factor and SAR1 in vesicular trafficking in
1121 plants. Biochim Biophys Acta **1664:** 9-30
1122 **Mori R, Toda T** (2013) The dual role of fission yeast Tbc1/cofactor C orchestrates microtubule
1123 homeostasis in tubulin folding and acts as a GAP for GTPase Alp41/Arl2. Molecular
1124 biology of the cell **24:** 1713-S1718
1125 **Nakai W, Kondo Y, Saitoh A, Naito T, Nakayama K, Shin HW** (2013) ARF1 and ARF4
1126 regulate recycling endosomal morphology and retrograde transport from endosomes
1127 to the Golgi apparatus. Mol Biol Cell **24:** 2570-2581

1128 **Nelson BK, Cai X, Nebenführ A** (2007) A multicolored set of in vivo organelle markers for
1129 co-localization studies in Arabidopsis and other plants. The Plant Journal **51:** 1126-
1130 1136
1131 **Newman LE, Zhou CJ, Mudigonda S, Mattheyses AL, Paradies E, Marobbio CM, Kahn**
1132 **RA** (2014) The ARL2 GTPase is required for mitochondrial morphology, motility, and
1133 maintenance of ATP levels. PLoS One **9:** e99270
1134 **Nielsen E** (2020) The Small GTPase Superfamily in Plants: A Conserved Regulatory Module
1135 with Novel Functions. Annual Review of Plant Biology **71:** 247-272
1136 **Niu F, Ji C, Liang Z, Guo R, Chen Y, Zeng Y, Jiang L** (2022) ADP-ribosylation factor D1
1137 modulates Golgi morphology, cell plate formation, and plant growth in Arabidopsis.
1138 Plant Physiol **190:** 1199-1213
1139 **Pasternak T, Tietz O, Rapp K, Begheldo M, Nitschke R, Ruperti B, Palme K** (2015)
1140 Protocol: an improved and universal procedure for whole-mount immunolocalization in
1141 plants. Plant Methods **11:** 50
1142 **Radcliffe PA, Vardy L, Toda T** (2000) A conserved small GTP-binding protein Alp41 is
1143 essential for the cofactor-dependent biogenesis of microtubules in fission yeast. FEBS
1144 Letters **468:** 84-88
1145 **Ritzenthaler C, Nebenführ A, Movafeghi A, Stussi-Garaud C, Behnia L, Pimpl P,**
1146 **Staehelin LA, Robinson DG** (2002) Reevaluation of the effects of brefeldin A on plant
1147 cells using tobacco Bright Yellow 2 cells expressing Golgi-targeted green fluorescent
1148 protein and COPI antisera. The Plant cell **14:** 237-261
1149 **Scheffzek K, Ahmadian MR, Kabsch W, Wiesmüller L, Lautwein A, Schmitz F,**
1150 **Wittinghofer A** (1997) The Ras-RasGAP Complex: Structural Basis for GTPase
1151 Activation and Its Loss in Oncogenic Ras Mutants. Science **277:** 333-339
1152 **Schneider CA, Rasband WS, Eliceiri KW** (2012) NIH Image to ImageJ: 25 years of image
1153 analysis. Nature Methods **9:** 671-675
1154 **Sharer JD, Kahn RA** (1999) The ARF-like 2 (ARL2)-binding protein, BART. Purification,
1155 cloning, and initial characterization. J Biol Chem **274:** 27553-27561
1156 **Sharer JD, Shern JF, Van Valkenburgh H, Wallace DC, Kahn RA** (2002) ARL2 and BART
1157 Enter Mitochondria and Bind the Adenine Nucleotide Transporter. Molecular Biology of
1158 the Cell **13:** 71-83
1159 **Singh MK, Richter S, Beckmann H, Kientz M, Stierhof Y-D, Anders N, Fäßler F, Nielsen**
1160 **M, Knöll C, Thomann A, Franz-Wachtel M, Macek B, Skriver K, Pimpl P, Jürgens**
1161 **G** (2018) A single class of ARF GTPase activated by several pathway-specific ARF-
1162 GEFs regulates essential membrane traffic in Arabidopsis. PLOS Genetics **14:**
1163 e1007795
1164 **Sohn EJ, Kim ES, Zhao M, Kim SJ, Kim H, Kim YW, Lee YJ, Hillmer S, Sohn U, Jiang L,**
1165 **Hwang I** (2003) Rha1, an Arabidopsis Rab5 homolog, plays a critical role in the
1166 vacuolar trafficking of soluble cargo proteins. Plant Cell **15:** 1057-1070
1167 **Stefano G, Renna L, Hanton SL, Chatre L, Haas TA, Brandizzi F** (2006) ARL1 plays a role
1168 in the binding of the GRIP domain of a peripheral matrix protein to the Golgi apparatus
1169 in plant cells. Plant Mol Biol **61:** 431-449
1170 **Stierhof YD, El Kasmi F** (2010) Strategies to improve the antigenicity, ultrastructure
1171 preservation and visibility of trafficking compartments in Arabidopsis tissue. Eur J Cell
1172 Biol **89:** 285-297
1173 **Sztul E, Chen P-W, Casanova JE, Cherfils J, Dacks JB, Lambright DG, Lee F-JS,**
1174 **Randazzo PA, Santy LC, Schürmann A, Wilhelmi I, Yohe ME, Kahn RA** (2019) ARF

1175 GTPases and their GEFs and GAPs: concepts and challenges. Molecular biology of
1176 the cell **30:** 1249-1271
1177 **Tzafrir I, McElver JA, Liu Cm C-m, Yang LJ, Wu JQ, Martinez A, Patton DA, Meinke DW**
1178 (2002) Diversity of TITAN functions in Arabidopsis seed development. Plant physiology
1179 **128:** 38-51
1180 **Ueda T, Yamaguchi M, Uchimiya H, Nakano A** (2001) Ara6, a plant-unique novel type Rab
1181 GTPase, functions in the endocytic pathway of *Arabidopsis thaliana*. The EMBO
1182 Journal **20:** 4730-4741
1183 **Valencia JP, Goodman K, Otegui MS** (2016) Endocytosis and Endosomal Trafficking in
1184 Plants. Annual Review of Plant Biology **67:** 309-335
1185 **Van Valkenburgh H, Shern JF, Sharer JD, Zhu X, Kahn RA** (2001) ADP-ribosylation factors
1186 (ARFs) and ARF-like 1 (ARL1) have both specific and shared effectors: characterizing
1187 ARL1-binding proteins. J Biol Chem **276:** 22826-22837
1188 **Veltel S, Kravchenko A, Ismail S, Wittinghofer A** (2008) Specificity of Arl2/Arl3 signaling is
1189 mediated by a ternary Arl3-effector-GAP complex. FEBS Letters **582:** 2501-2507
1190 **Vernoud V, Horton AC, Yang Z, Nielsen E** (2003) Analysis of the small GTPase gene
1191 superfamily of Arabidopsis. Plant Physiol **131:** 1191-1208
1192 **Volpicelli-Daley LA, Li Y, Zhang CJ, Kahn RA** (2005) Isoform-selective effects of the
1193 depletion of ADP-ribosylation factors 1-5 on membrane traffic. Mol Biol Cell **16:** 4495-
1194 4508
1195 **Waese J, Fan J, Pasha A, Yu H, Fucile G, Shi R, Cumming M, Kelley LA, Sternberg MJ,**
1196 **Krishnakumar V, Ferlanti E, Miller J, Town C, Stuerzlinger W, Provart NJ** (2017)
1197 ePlant: Visualizing and Exploring Multiple Levels of Data for Hypothesis Generation in
1198 Plant Biology. The Plant Cell **29:** 1806-1821
1199 **Wang J, Cai Y, Miao Y, Lam SK, Jiang L** (2009) Wortmannin induces homotypic fusion of
1200 plant prevacuolar compartments*. Journal of Experimental Botany **60:** 3075-3083
1201 **Wang Y, Liu F, Ren Y, Wang Y, Liu X, Long W, Wang D, Zhu J, Zhu X, Jing R, Wu M, Hao**
1202 **Y, Jiang L, Wang C, Wang H, Bao Y, Wan J** (2016) GOLGI TRANSPORT 1B
1203 Regulates Protein Export from the Endoplasmic Reticulum in Rice Endosperm Cells.
1204 The Plant Cell **28:** 2850-2865
1205 **Waterhouse AM, Procter JB, Martin DM, Clamp M, Barton GJ** (2009) Jalview Version 2--a
1206 multiple sequence alignment editor and analysis workbench. Bioinformatics **25:** 1189-
1207 1191
1208 **Wright J, Kahn RA, Sztul E** (2014) Regulating the large Sec7 ARF guanine nucleotide
1209 exchange factors: the when, where and how of activation. Cellular and Molecular Life
1210 Sciences **71:** 3419-3438
1211 **Zhang CJ, Rosenwald AG, Willingham MC, Skuntz S, Clark J, Kahn RA** (1994) Expression
1212 of a dominant allele of human ARF1 inhibits membrane traffic in vivo. J Cell Biol **124:**
1213 289-300
1214 **Zhang H, Yang Z, Lin T, Wu Y, Zou T, yang J, Zhang Y** (2018) ARL2 regulates trafficking
1215 and expression of isoprenylated proteins and is crucial for development of
1216 photoreceptor outer segments. Investigative Ophthalmology & Visual Science **59:** 963-
1217 963
1218 **Zhou C, Cunningham L, Marcus AI, Li Y, Kahn RA** (2006) Arl2 and Arl3 regulate different
1219 microtubule-dependent processes. Mol Biol Cell **17:** 2476-2487

1220

Figures

Characterization of the small *Arabidopsis thaliana* GTPase and ADP-ribosylation factor-like 2 protein TITAN 5

Inga Mohr[1], Amin Mirzaiebadizi[2], Sibaji K. Sanyal[1], Pichaporn Chuenban[1], Mohammad R. Ahmadian[2], Rumen Ivanov[1] and Petra Bauer[1,3]

[1]Institute of Botany, Heinrich Heine University, 40225 Düsseldorf, Germany.
[2]Institute of Biochemistry and Molecular Biology II, Medical Faculty and University Hospital Düsseldorf, Heinrich Heine University, Düsseldorf, Germany
[3]Cluster of Excellence on Plant Sciences, Heinrich Heine University, 40225 Düsseldorf,
Germany

Figure 1

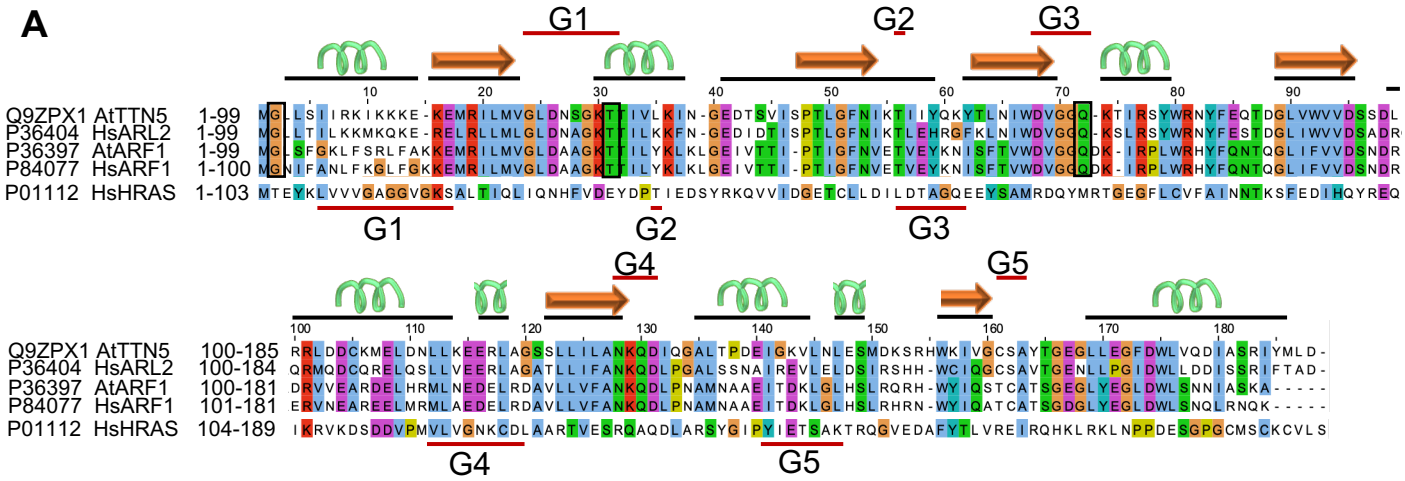
A
G1
G2
G3
Q9ZPX1 AtTTN5 1-99
P36404 HsARL2 1-99
P36397 AtARF1 1-99
P84077 HsARF1 1-100
P01112 HsHRAS 1-103
G1
G2
G3
G4
G5
Q9ZPX1 AtTTN5 100-185
P36404 HsARL2 100-184
P36397 AtARF1 100-181
P84077 HsARF1 101-181
P01112 HsHRAS 104-189
G4
G5

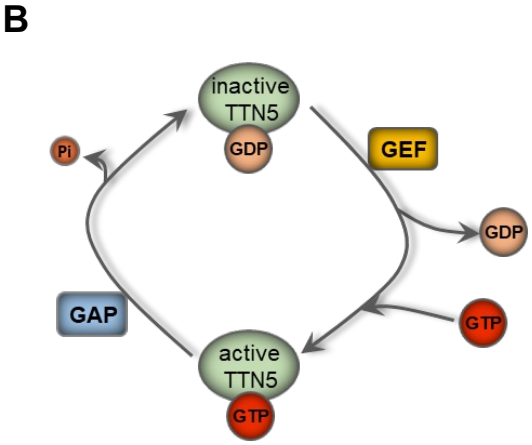
B
inactive TTN5
GDP
Pi
GEF
GDP
GTP
GAP
active TTN5
GTP

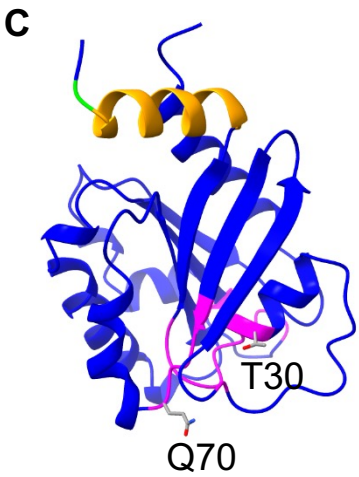
C
T30
Q70

Figure 1: TTN5, a functional small ARF-like GTPase with nucleotide exchange capacity. (A), Sequence alignment of TTN5 with its human homolog ARL2, Arabidopsis, human ARF1, and human HRAS created with Jalview (Waterhouse et al., 2009). The conserved G-motifs (G1-G5; indicated by red lines) are defined for the TTN5 and HRAS sequence. The secondary structure of TTN5 is depicted by red lines and corresponding cartoon (α-helix in green; β-sheet in orange). Here mentioned conserved residues in ARF/ARL proteins are highlighted by boxes; Gly-2, and mutated Thr-30 and Gln-70. $TTN5^{T30N}$ is expected to have a low nucleotide exchange capacity, while $TTN5^{Q70L}$ is expected to have a low GTPase hydrolysis activity. (B), Model of the predicted GTPase nucleotide exchange and hydrolysis cycle of TTN5. TTN5 switches from an inactive GDP-loaded form to an active GTP-loaded one. GDP to GTP nucleotide exchange and GTP hydrolysis may be aided by a guanidine exchange factor (GEF) and a GTPase-activating protein (GAP). (C), Predicted protein structural model of TTN5; magenta, marks the GTP-binding pocket; N-terminal amphipathic helix is highlighted in orange; conserved Gly-2 in green; T30 and Q70, mutagenized in this study, shown in sticks. The model was generated with AlphaFold (Jumper et al., 2021), and adaptation was done with UCSF ChimeraX 1.2.5 (Goddard et al., 2018).

Figure 2

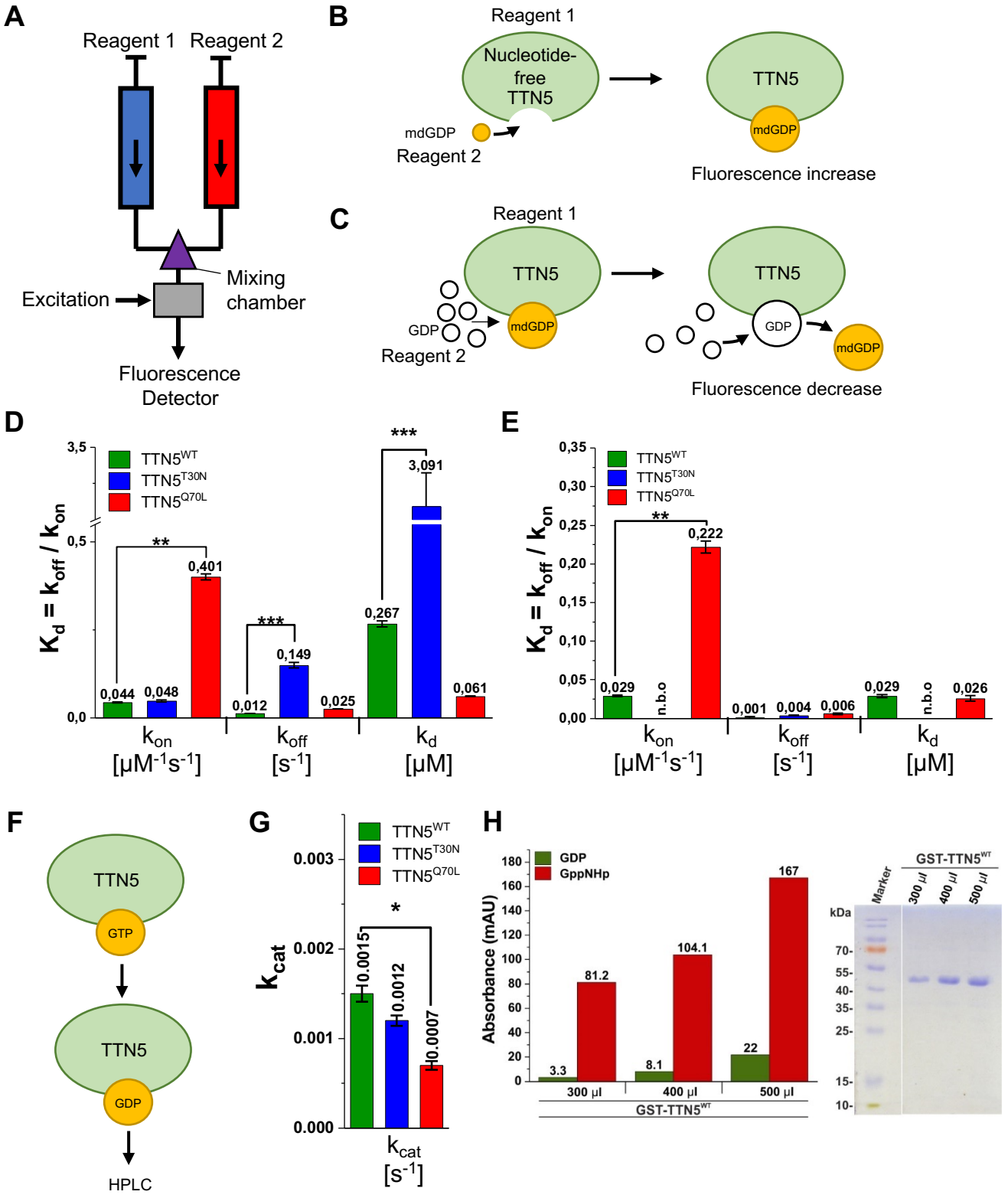
A
Reagent 1
Reagent 2
Mixing chamber
Excitation
Fluorescence Detector
B
Reagent 1
Nucleotide-free TTN5
mdGDP
Reagent 2
TTN5
mdGDP
Fluorescence increase
C
Reagent 1
TTN5
GDP
mdGDP
Reagent 2
TTN5
GDP
mdGDP
Fluorescence decrease
D
TTN5WT
TTN5T30N
TTN5Q70L
Kd = koff / kon
0,044
0,048
0,401
0,012
0,149
0,025
0,267
3,091
0,061
kon [μM-1s-1]
koff [s-1]
kd [μM]
E
TTN5WT
TTN5T30N
TTN5Q70L
Kd = koff / kon
0,029
n.b.o
0,222
0,001
0,004
0,006
0,029
n.b.o
0,026
kon [μM-1s-1]
koff [s-1]
kd [μM]
F
TTN5
GTP
TTN5
GDP
HPLC
G
TTN5WT
TTN5T30N
TTN5Q70L
kcat
0.0015
0.0012
0.0007
kcat [s-1]
H
GDP
GppNHp
Absorbance (mAU)
3.3
81.2
8.1
104.1
22
167
300 µl
400 µl
500 µl
GST-TTN5WT
Marker
GST-TTN5WT
300 µl
400 µl
500 µl
kDa
70-
55-
40-
35-
25-
15-
10-

Figure 2: Biochemical properties of TTN5 proteins suggest that TTN5 is present in a GTP-loaded active form in cells. (A), Schematic illustration of the stopped-flow fluorescence device for monitoring the nucleotide-binding kinetics of the purified TTN5 protein heterologously expressed in bacteria (Supplementary Figure S2A-D). It consists of two motorized, thermostated syringes, a mixing chamber, and a fluorescence detector. Two different reagents 1 and 2 are rapidly mixed and transferred to a fluorescence detection cell within 4 ms. One of the reagents must contain a fluorescent reporter group. Here, mdGDP and mGppNHp were used to mimic GDP and GTP. (B), Schematic illustration of the nucleotide association. Nucleotide-free TTN5 (reagent 1; preparation see Supplementary Figure S2E) was rapidly mixed with mdGDP (reagent 2). A fluorescence increase is expected upon association of mdGDP with TTN5. Similar measurements are performed with mGppNHp instead of mdGDP. (C), Schematic illustration of the intrinsic nucleotide exchange. mdGDP-bound TTN5 (reagent 1) is mixed with a molar excess of GDP (reagent 2). A fluorescence decrease is expected upon mdGDP dissociation from TTN5 and binding of free GDP. Similar measurements are performed with mGppNHp. (D-E), Kinetics of association and dissociation of fluorescent nucleotides with TTN5 proteins (WT, $TTN5^{T30N}$, $TTN5^{Q70L}$) are illustrated as bar charts. The association of mdGDP (0.1 µM) or mGppNHp (0.1 µM) with increasing concentration of $TTN5^{WT}$, $TTN5^{T30N}$, and $TTN5^{Q70L}$ was measured using a stopped-flow device (see A, B; data see Supplementary Figure S3A-F, S4A-E). Association rate constants (k_{on} in $\mu M^{-1}s^{-1}$) were determined from the plot of increasing observed rate constants (k_{obs} in s^{-1}) against the corresponding concentrations of the TTN5 proteins. Intrinsic dissociation rates (k_{off} in s^{-1}) were determined by rapidly mixing 0.1 µM mdGDP-bound or mGppNHp-bound TTN5 proteins with the excess amount of unlabeled GDP (see A, C, data see Supplementary Figure S3G-I, S4F-H). The nucleotide affinity (dissociation constant or K_d in µM) of the corresponding TTN5 proteins was calculated by dividing k_{off} by k_{on}. When mixing mGppNHp with nucleotide-free $TTN5^{T30N}$, no binding was observed (n.b.o.) under these experimental conditions. (F-G), GTP hydrolysis of TTN5 proteins determined by HPLC. (F), Schematic illustration of the GTP hydrolysis measurement. (G), GTP-bound TTN5 proteins (100 µM) were incubated at room temperature at different time points before injecting them on a reversed-phase HPLC system. Evaluated data (data see Supplementary Figure S5) resulted in the determination of the GTP hydrolysis rates (k_{cat}) illustrated as bar charts. (H), TTN5 accumulated in a GTP-loaded active form. GST-$TTN5^{WT}$ (46.5 kDa) was purified from bacterial cell lysates at three different volumes in the presence of 0.1 µM unbound free GppNHp using glutathione beads. The nucleotide contents and the protein purities were determined by HPLC and Coomassie Blue-stained SDS-polyacrylamide gel electrophoresis. The presence of much higher amounts of GppNHp-bound versus GDP-bound GST-TTN5 protein indicates that TTN5 rapidly exchanged bound nucleotide und accumulated in this state.

Figure 3

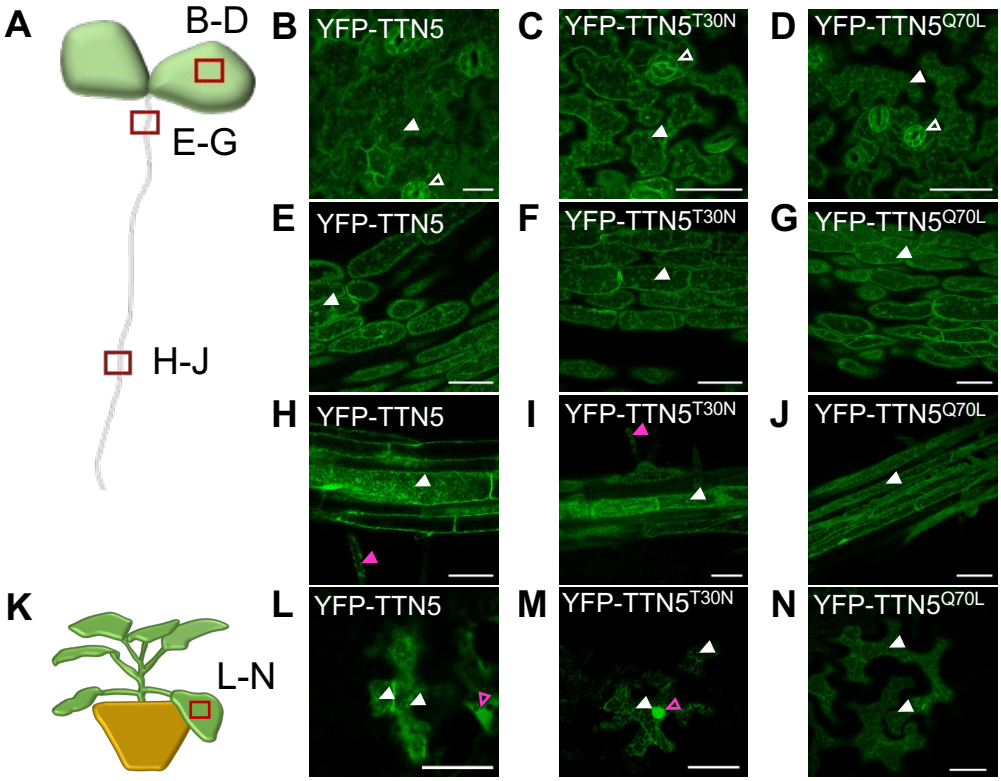
A
B-D
E-G
H-J
K
L-N
B
YFP-TTN5
C
YFP-TTN5T30N
D
YFP-TTN5Q70L
E
YFP-TTN5
F
YFP-TTN5T30N
G
YFP-TTN5Q70L
H
YFP-TTN5
I
YFP-TTN5T30N
J
YFP-TTN5Q70L
L
YFP-TTN5
M
YFP-TTN5T30N
N
YFP-TTN5Q70L

Figure 3: TTN5 was present in punctate structures. Microscopic observations were made in a plane underneath the plasma membrane at the cell peripheries. (A), Schematic representation of an Arabidopsis seedling. Images were taken at three different positions of the seedlings and imaged areas are indicated by a red rectangle. (B-J), YFP-TTN5, YFP-TTN5^{T30N} and YFP-TTN5^{Q70L} protein localization in Arabidopsis seedlings *via* fluorescent confocal microscopy. (B-D), YFP-TTN5 and its two mutant variants YFP-TTN5^{T30N} and YFP-TTN5^{Q70L} were observed in stomata (indicated by empty white arrowhead) and in the epidermis of cotyledons in punctate structures (indicated by filled white arrowhead). (E-G), Localization in the hypocotyls showed the same pattern of punctate structures. (H-J), YFP-TTN5 and its two mutant variants YFP-TTN5^{T30N} and YFP-TTN5^{Q70L} were present in punctate structures in the root hair zone and in root hairs (indicated by filled magenta arrowhead). (K), Schematic representation of a *N. benthamiana* plant, used for leaf infiltration for transient expression. Imaged areas are indicated by a red rectangle. (L-N), YFP-TTN5 signals in *N. benthamiana* leaf epidermal cells. YFP-TTN5 and its two mutant variants YFP-TTN5^{T30N} and YFP-TTN5^{Q70L} are present in punctate structures (indicated by white arrowheads) and in the nucleus (indicated by empty magenta arrowheads). Scale bar 50 µm.

Figure 4

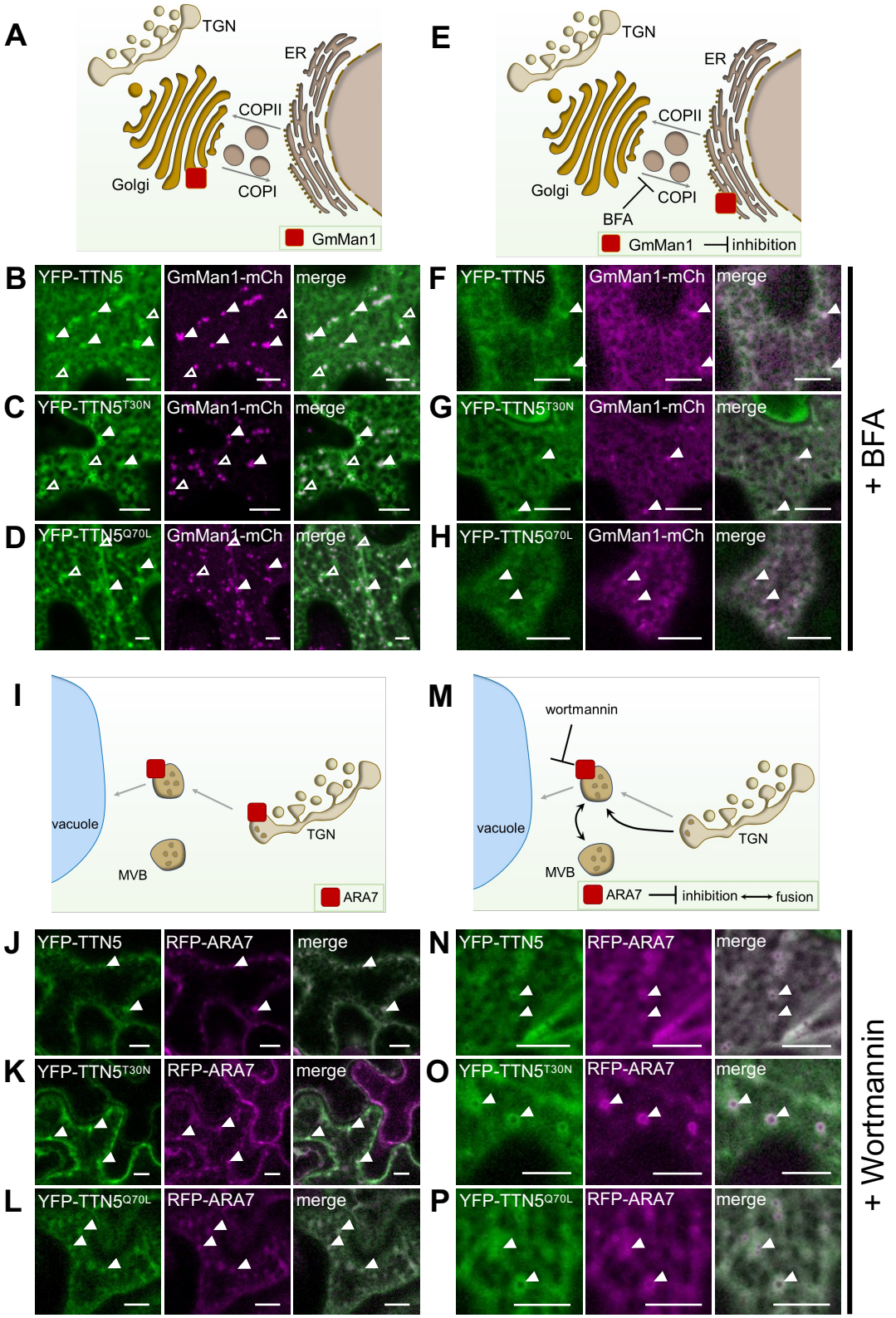
A
TGN
ER
COPII
Golgi
COPI
GmMan1
E
TGN
ER
COPII
Golgi
COPI
BFA
GmMan1
inhibition
B
YFP-TTN5
GmMan1-mCh
merge
C
YFP-TTN5T30N
GmMan1-mCh
merge
D
YFP-TTN5Q70L
GmMan1-mCh
merge
F
YFP-TTN5
GmMan1-mCh
merge
G
YFP-TTN5T30N
GmMan1-mCh
merge
H
YFP-TTN5Q70L
GmMan1-mCh
merge
+ BFA
I
vacuole
MVB
TGN
ARA7
M
wortmannin
vacuole
MVB
TGN
ARA7
inhibition
fusion
J
YFP-TTN5
RFP-ARA7
merge
K
YFP-TTN5T30N
RFP-ARA7
merge
L
YFP-TTN5Q70L
RFP-ARA7
merge
N
YFP-TTN5
RFP-ARA7
merge
O
YFP-TTN5T30N
RFP-ARA7
merge
P
YFP-TTN5Q70L
RFP-ARA7
merge
+ Wortmannin

Figure 4: YFP-TTN5 associated with the endomembrane system in *N. benthamiana* leaf epidermal cells. YFP-TTN5 and its variants YFP-TTN5^{T30N} and YFP-TTN5^{Q70L} were localized in *N. benthamiana* leaf epidermal cells with specific markers *via* fluorescent confocal microscopy. (A), Schematic representation of GmMan1 localization at the *cis*-Golgi site. (B-D), Partial colocalization of YFP-TTN5 proteins with the Golgi marker GmMan1-mCherry at *cis*-Golgi stacks (filled white arrowheads). Additionally, YFP-TTN5 constructs were expressed individually in vesicular-like structures (empty white arrowheads). (E), Schematic representation of GmMan1 localization at the ER after redistribution of the Golgi to the ER upon brefeldin A (BFA) treatment. (F-H), Redistribution of Golgi stacks was induced by BFA treatment. GmMan1-mCherry and YFP-TTN5 constructs were present in the ER and in coexpressing punctate structures. (I), Schematic representation of ARA7 localization at the *trans*-Golgi network (TGN) and multi-vesicular bodies (MVBs). (J-L), Colocalization of YFP-TTN5 proteins with the MVB marker RFP-ARA7. (M), Schematic representation of ARA7 localization in swollen MVBs upon wortmannin treatment. (N-P), MVB swelling was obtained by wortmannin treatment. ARA7-RFP was colocalizing with YFP-TTN5 constructs in these swollen MVBs. Chemical treatment-induced changes were imaged after 25 min incubation. Colocalization is indicated with filled arrowheads, YFP-tagged construct expression alone with empty ones. Corresponding colocalization analysis data is presented in Supplementary Figure S8. Scale bar 10 µm.

Figure 5

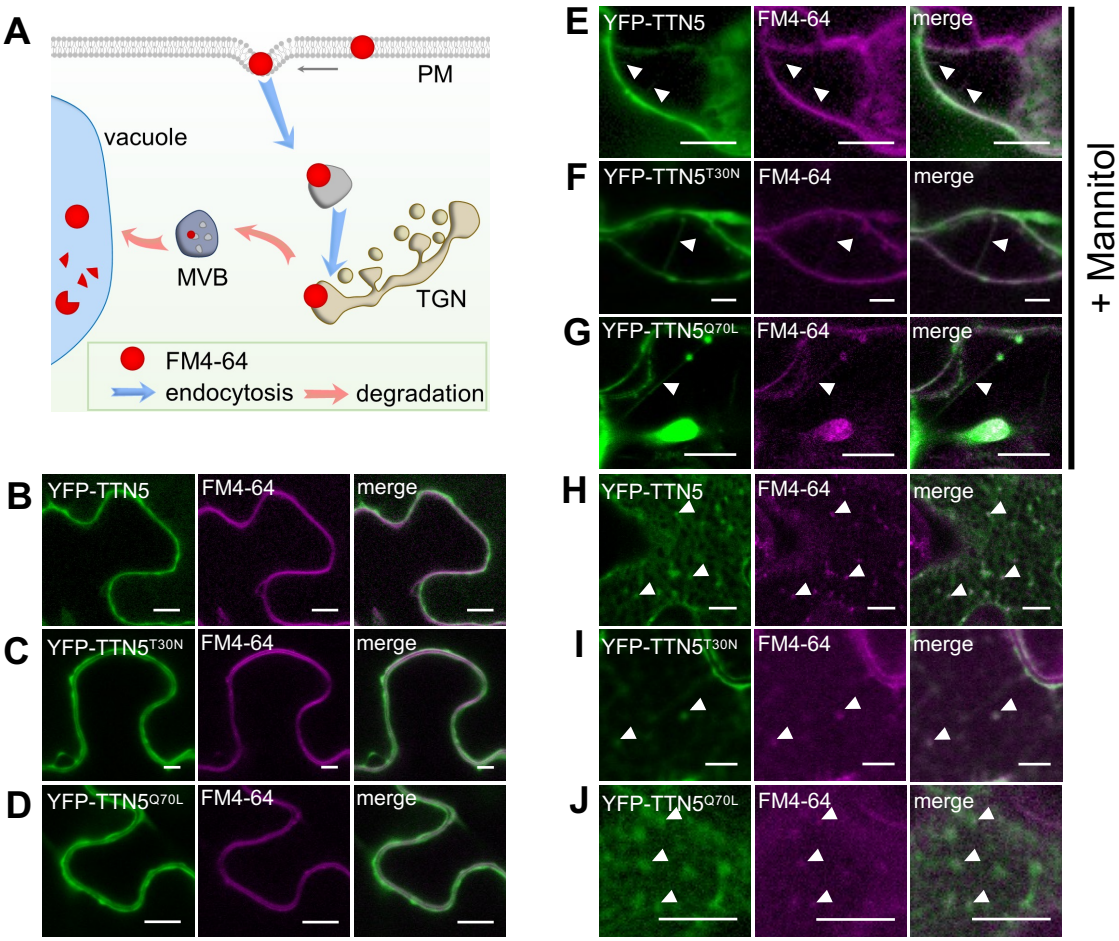
A
PM
vacuole
MVB
TGN
FM4-64
endocytosis
degradation
B
YFP-TTN5
FM4-64
merge
C
YFP-TTN5T30N
FM4-64
merge
D
YFP-TTN5Q70L
FM4-64
merge
E
YFP-TTN5
FM4-64
merge
F
YFP-TTN5T30N
FM4-64
merge
G
YFP-TTN5Q70L
FM4-64
merge
+ Mannitol
H
YFP-TTN5
FM4-64
merge
I
YFP-TTN5T30N
FM4-64
merge
J
YFP-TTN5Q70L
FM4-64
merge

Figure 5. YFP-TTN5 colocalized with endocytosed plasma membrane material. (A), Schematic representation of FM4-64 plasma membrane localization and endocytosis. (B-J), YFP-tagged TTN5 and mutant forms YFP-TTN5^{T30N} andYFP-TTN5^{Q70L} were localized in *N. benthamiana* leaf epidermal cells together with the plasma membrane dye FM4-64 *via* fluorescent confocal microscopy. (B-D), YFP-TTN5, YFP-TTN5^{T30N} and YFP-TTN5^{Q70L} colocalized with FM4-64 at the plasma membrane. (E-G), YFP-TTN5 protein plasma membrane localization was tested by mannitol-induced (1 M) plasmolysis. The formation of Hechtian strands is indicated with filled arrowheads. (H-J), Internalized FM4-64 was present in YFP-TTN5 and the respective GTPase-variant coexpressing vesicle-like structures. Colocalization is indicated with filled arrowheads. Scale bar 10 µm.